

Decoding the IGF1 Signaling Gene Regulatory Network Behind Alveologenesis from A Mouse Model of Bronchopulmonary Dysplasia

Gao F¹, Li C¹, Smith SM¹, Peinado N¹, Kohbodi G¹, Tran E^{2,3}, Loh E⁴, Li W⁵, Borok Z⁶ and Minoo P^{1,7}

1- Division of Neonatology, Department of Pediatrics, LAC+USC Medical Center and Children's Hospital Los Angeles, Los Angeles, CA 90033, USA.

2- Norris Comprehensive Cancer Center, Keck School of Medicine, USC, Los Angeles, CA 90033, USA.

3- Department of Biochemistry and Molecular Medicine, Keck School of Medicine, USC, Los Angeles, CA 90033, USA.

4- Norris Medical Library, University of Southern California, Los Angeles, CA 90033, USA.

5- Department of Pediatrics, Jiangsu Provincial Hospital of Traditional Chinese Medicine, Nanjing 210004, China.

6- Division of Pulmonary, Critical Care and Sleep Medicine, Department of Medicine, University of California, San Diego, La Jolla, CA 92093, USA.

7- Division of Pulmonary, Critical Care and Sleep Medicine and Hastings Center for Pulmonary Research, Keck School of Medicine of University of Southern California, Los Angeles, CA, 90033, USA.

*Authors for correspondence: fremontgao@gmail.com and minoo@usc.edu

Summary

Lung development is precisely controlled by underlying Gene Regulatory Networks (GRN). Disruption of genes in the network can interrupt normal development and cause diseases such as bronchopulmonary dysplasia (BPD), a chronic lung disease in preterm infants with morbid and sometimes lethal consequences that is characterized by lung immaturity and reduced alveolarization.

Here, we generated a transgenic mouse exhibiting a moderate severity BPD phenotype by blocking IGF1 signaling in secondary crest myofibroblasts (SCMF) at the onset of alveologenesis. Using approaches mirroring the construction of the model GRN in sea urchin's development, we constructed the IGF1 signaling network underlying alveologenesis using this mouse model that phenocopies BPD. The constructed GRN, consisting of 43 genes, provides a bird's-eye view of how the genes downstream of IGF1 are regulatorily connected. The GRN also reveals a mechanistic interpretation of how the effects of IGF1 signaling are transduced within SCMF from its specification genes to its effector genes and then from SCMF to its neighboring alveolar epithelial cells with Wnt5a and Fgf10 signaling as the bridge. Consistently, blocking of Wnt5a signaling in mice phenocopies BPD as inferred by the network. A comparative study on human samples suggests that a GRN of similar components and wiring underlies human BPD.

Our network view of alveologenesis is transforming our perspective to understand and treat BPD. The new perspective calls for the construction of the full signaling GRN underlying alveologenesis, upon which targeted therapies for this neonatal chronic lung disease can be viably developed.

Introduction

Development is precisely controlled by the genetic program encoded in the genome and is governed by genetic interactions (Davidson et al., 2002; Levine and Davidson, 2005). Elucidating the network of interactions among genes that govern morphogenesis through development is one of the core challenges in contemporary functional genomics research (Przybyla and Gilbert, 2021). These networks are known as developmental gene regulatory networks (GRN) which are key to understanding the developmental processes with integrative details and mechanistic perspective. Over the past few decades, great advances have been made in decoding these networks in classical model systems (i.e. Dequeant and Pourquie, 2008; Longabaugh et al., 2017; Olson, 2006; Satou et al., 2009; Sauka-Spengler and Bronner-Fraser, 2008), as well as the in-depth understanding of the general design principles of these networks in development and evolution (Carre et al., 2017; Davidson, 2010; Erwin and Davidson, 2009; Gao and Davidson, 2008; Lim et al., 2013; Peter and Davidson, 2009). Highlighted among them is the sea urchin developmental GRN, the most comprehensive and authenticated network constructed to date (Peter and Davidson, 2017).

Disruption of any gene in the network could interrupt normal development and conceivably cause disease. Some diseases are caused by single gene disorders while others are complex and multi-factorial such as bronchopulmonary dysplasia (BPD), a common cause of morbidity and mortality in preterm infants with their lungs characterized by arrested alveolar development with varied severity (Jain and Bancalari, 2014; Jobe, 1999; Short et al., 2007). Both prenatal insults and postnatal injury increase the risk of BPD. The multifactorial etiology of BPD has made the development of therapies a unique challenge, and currently no effective treatment exists to prevent or cure this debilitating disease.

In recent clinical trials, therapy with recombinant human insulin like growth factor 1 (rhIGF1) protein showed initial promise for BPD, but significant limitations did not allow further clinical trials (Ley et al., 2019; Seedorf et al., 2020). One impediment to further development of IGF1 as a therapy is lack of comprehensive information regarding the precise role of the IGF1 signaling pathway in alveologenesis.

Alveolar development is a highly complex process that is driven by multiple signaling pathways including Tgfb, Shh, Wnt, Pdgf, Vegf, Hgf, Notch, Bmp and IGF1 (Juul et al., 2020; Nabhan et al., 2018; Tsao et al., 2016; Verheyden and Sun, 2020; Wu and Tang, 2021; Zepp and Morrissey, 2019). Igf1 and Igf1R expression is found throughout fetal lung development and fluctuates at different stages. Both Igf1 and Igf1R expression is significantly reduced in BPD lungs (Hellstrom et al., 2016; Lofqvist et al., 2012; Yilmaz et al., 2017), suggesting a potential role in pathogenesis of BPD. The function of Igf1 and Igf1R has been examined in their respective constitutive and conditional knockout mice, but their specific function during alveologenesis has not been examined (Epauld et al., 2012; Lopez et al., 2016; Lopez et al., 2015). A recent study found interruption in IGF1 signaling compromised mechanosignaling and interrupted alveologenesis (He et al., 2021).

In our study here, we found Igf1 and Igf1R are primarily expressed in SCMF in postnatal mouse lung. As a result, we interrupted IGF1 signaling in SCMF by inactivation of Igf1R at the onset of alveologenesis in postnatal day 2 (PN2) mouse neonates and analyzed the resulting phenotypes. Inactivation of Igf1R resulted in mutant lungs with simplified and immature alveolar structure reminiscent of the human BPD of moderate severity (Short et al., 2007). We reasoned that the phenotype caused by inactivation of IGF1 in SCMF reflects interruption in the genetic program downstream of IGF1 signaling that drives the normal functions of SCMF in the process of alveologenesis. Alterations in SCMF may further impact specification/differentiation of other

key cell types, particularly the alveolar epithelial cells. We aim to decode the genes and their interactions behind this underlying genetic program.

Taking advantage of the high throughput next generation sequencing, people have been trying to build GRNs by computational analysis using wild type gene expression data (i.e. Jia et al., 2017; Xu et al., 2012). Currently, the most reliable way is still to build GRN experimentally on data from perturbation analyses.

Genes we particularly focus on are the regulatory genes. These genes decide the outcome of a GRN as they regulate and control other genes' expression forming a regulatory circuitry of varied hierarchy with structural and cellular genes as their terminal targets (Davidson, 2010; Erwin and Davidson, 2009). Their functions are defined by their logical control over the circuitry's operation and their synergetic biological effects are manifested by the effector genes under the circuitry (Peter and Davidson, 2009; Peter et al., 2012).

We followed the protocol similar to that used in construction of the sea urchin GRN (Materna and Oliveri, 2008): regulatory genes were selected at the transcriptomic scale from LungMAP database (www.lungmap.net) where their expression during alveologenesis were reported; the cellular expression patterns of these genes were annotated on lungMap scRNAseq data for the screen of SCMF genes; the regulatory interactions among these genes were examined from in vivo and in vitro perturbations; and cellular communications were determined by secretome-receptome analysis. Combining these data, we constructed the IGF1 signaling gene regulatory network underlying alveologenesis from this mouse model of human BPD phenocopy.

Our GRN work on alveologenesis represents a transformative view of how to understand and perhaps even design future preventive and therapeutic strategies for treatment of BPD.

Results

Postnatal Expression of Igf1 and Igf1r in the lung.

To define the expression pattern of Igf1 and Igf1r during early postnatal lung development, we performed RT-PCR using total lung RNA from embryonic day E18 to postnatal day PN30. The analysis showed Igf1 is expressed dynamically during development peaking at the onset of alveologenesis and progressively decreasing during this process (Fig.1A). The expression pattern of *Igf1r* was biphasic, initially displaying an overlap with *Igf1* in early alveologenesis with a subsequent peak occurring on PN21 (Fig.1B).

Hedgehog responsive alveolar myofibroblasts, which we term secondary crest myofibroblasts (SCMF), are required for alveologenesis, a process characterized by alveolar secondary crest formation (Branchfield et al., 2016; Li et al., 2015; Li et al., 2020b). RNAscope showed highly overlapping localization of *Igf1/Igf1r* and *Pdgfra*, a SCMF marker gene (Li et al., 2019a; Li et al., 2018) (Fig.1C), indicating SCMF as a principal cellular site of *Igf1* and *Igf1r* expression in lungs undergoing alveologenesis.

Mesodermal-specific Inactivation of Igf1 and Igf1r.

As SCMF are derived from the lung mesenchyme early in lung development and *Dermo1* is activated specifically at the onset of mesodermal lineage specification (Li et al., 2008), we used *Dermo1-cre* (*Dcre*) to inactivate *Igf1* or *Igf1r* separately and specifically in the mesodermal lineages and examined the mutant lung phenotype during embryonic and postnatal development (SFig.1A).

Loss of *Igf1* or *Igf1r* in mesodermal progenitors using floxed alleles of these genes decreased their mRNA by approximately two folds (SFig.1B). In consistent with previous reports (Epaud et al., 2012; Lopez et al., 2015), loss of body weight was observed in our *Igf1r* mutant pups (SFig.1C&D).

The *Dcre;Igf1r-f/f* mutant has clearly visible lung defects, with thickened saccular walls at E18, dilated sacculi and severely reduced number of secondary crests at PN14 that persists to PN30 (SFig.1E). Similar defects of less severity were observed in the *Dcre;Igf1-f/f* mutant (SFig.1F). However, due to the timing of *Dermo1-cre* activation, it is difficult to determine whether the impact of *Igf1r* on alveologenesis occurs postnatally or is a carryover impact of events occurring prior to onset of alveologenesis.

Postnatal inactivation of Igf1r in SCMF profoundly arrests alveologenesis.

Using *Gli1-creERT2* (*Gcre*), which targets SCMF (Li et al., 2015), we inactivated floxed alleles of *Igf1r* on PN2 at the onset of alveologenesis (Fig.2A). Inactivation of *Igf1r* was validated by genotyping (SFig.2A), and its downregulation verified by RT-PCR with RNA from both whole lung and FACS-isolated SCMF (SFig.2B). The extent of overlap between Cre-induced green fluorescent protein (GFP) and Eln, a marker for SCMF, indicated efficient recombination (SFig.2C). The mutant mice were slightly runted compared to controls (SFig.2D).

Histology of multiple *Gcre;Igf1r-f/f* lungs at the timepoints PN7, PN14 and PN30, revealed a phenotype of profoundly arrested alveolar formation as measured by mean linear intercept (MLI) (Fig.2B). In addition, ImageJ analysis showed decreased perimeter/area ratio of airspace (Peri/Area) and the number of airspaces per unit of area (# of Airspace/Area), all consistent with the alveolar hypoplasia phenotype in the mutant lungs (Fig.2B, SFig.2E,F). The largest deviation between control and mutant in these measurements occurred at PN14, which marks

the midpoint in the alveologenesis phase. Still, the severity of hypoplasia here is eclipsed by that seen in *Gcre;Tgfbf-f/f* induced BPD phenocopies (Gao et al., 2022).

Immunohistochemical analysis revealed no significant gross changes between the control and mutant lungs in either proliferation or apoptosis (SFig.2G). Similarly, examination of specific markers for various lung alveolar cell lineages including the mesenchyme (ELN, TPM1), myofibroblasts (ACTA2, PDGFRA), endothelial cells (EMCN), lipofibroblasts (ADRP), epithelial cells (NKX2.1, SFTPC, HOPX) and pericytes (NG2) did not reveal significant differences (Fig.2C, SFig.2H). Nonetheless, it was observed in the mutant lungs the deposition of elastin seemed aggregated at the secondary crest tips and the number of AT1 and AT2 cells were reduced (Fig.2C). The altered elastin deposition has been reported in previous studies (He et al., 2021; Li et al., 2019a), but whether this alteration is the cause or the consequence of the impaired alveolar formation remains unknown.

To examine the genetic changes in *Gcre;Igf1r-f/f* mutant lungs, we tested two selected groups of genes: lung signature (SFig.2J) and angiogenesis (SFig.2K) genes. This analysis showed significant alterations in a few genes including *Fgf10*, *Igf1r* and *Pdgfra* in the mutant lungs. It is noteworthy that RNA used in the test was from whole lung tissue, while inactivation of *Igf1r* by *Gcre* was only targeted to SCMF. To determine the cell specific impacts of *Igf1r* inactivation, we characterized gene expression in FACS sorted cells in the following studies.

Identification of SCMF genes altered in mouse lungs of BPD phenotype.

Both GFP+ (SCMF) and Tomato+ (non-SCMF) cells were isolated by FACS from lungs dissected from *Gcre;mTmG* (control) and *Gcre;mTmG;Igf1r-f/f* (mutant) mice. Using the sorted cells, we compared gene expression between them to identify genes enriched in SCMF and those altered in SCMF and non-SCMFs in mutant lungs (Fig.3A, SFig.3A).

Our analysis didn't focus on the components of the pathway itself which are self-conserved and usually tissue-independent (Pires-daSilva and Sommer, 2003), and instead was directed at identifying genes downstream of the pathway, especially the regulatory genes through which the developmental GRN is specified (Erwin and Davidson, 2009). 47 genes known to encode signaling molecules and transcription factors were screened from the LungMAP transcriptomic database (www.lungmap.net), where they were indicated to be expressed from SCMF between PN3 to PN14 in the mouse developmental window (Supplemental Table 1). Expression of the selected genes, together with 15 known SCMF cell markers and 3 non-SCMF genes (negative control), were examined and compared by Realtime RT-PCR using RNA from the sorted cells.

Three criteria were applied to identify *Igf1* signaling targets within SCMF: (1) Functionally active in SCMF with its $\Delta\text{CT} \leq 9$ (relative to *Gapdh* in Ctrl_GFP, Supplemental Table 1), that is equivalent to ≥ 10 copies of transcripts per cell (copies of *Gapdh* transcripts per cell based on Barber et al., 2005); (2) highly enriched in SCMF with FC ≥ 10 , $p \leq 0.05$ (Ctrl_GFP vs Ctrl_Tomato, Fig.3B left column, Supplemental Table 1); (3) significantly altered with FC ≥ 2 , $p \leq 0.05$ (Mut_GFP vs Ctrl_GFP, Fig.3B right column, Supplemental Table 1).

Nineteen genes were identified that met all these 3 criteria (genes highlighted in red in the first column in Supplemental Table 1). Spatial localization of a select number of these genes including *Foxd1*, *Sox8*, *Tbx2*, *Bmper*, *Actc1*, *Wnt5a* and *Fgf10* in SCMF was validated by IHC (Fig.3C, SFig.3B) or RNAscope (Fig.3D).

Regulation of the latter 19 genes by *Igf1* signaling was illustrated on Biotapestry (Longabaugh, 2012) as displayed in Fig.3E. Of note, all connections were drawn directly from the signaling,

whereas the regulation may happen indirectly through the cross regulation among these genes (to be examined below).

The constructed link map points to IGF1 signaling as a positive regulator of 17 out of the 19 putative downstream genes (Fig.3E). Based on their molecular and cellular functions, the 19 genes can be stratified into two separate groups. One group is comprised of regulatory genes encoding transcription factors (*Gli1*, *Foxd1*, *Tbx2*, *Sox8*, *Dermo1*, *Rxra*) and signaling molecules (*Fgf10*, *Wnt5a*, *Bmper*, *Cyr61*, *Pdgfra*). The second group is comprised of *Acta2*, *Actc1*, *BGN*, *Des*, *Eln*, *Cnn1*, *FN1*, and *TNC*, representing genes that encode structural & cellular molecules. Based on the GRN's hierarchal design (Erwin and Davidson, 2009), it is most likely that IGF1 signaling first targets the regulatory genes, referred to as SCMF specifiers, whose expression subsequently targets the downstream structural and cellular genes in SCMF, heretofore called SCMF effectors.

Cross regulation of altered SCMF genes in the mouse BPD phenocopy model.

Within the inventory of altered SCMF genes, as defined above, are one transcription factor, *Foxd1*, one of the most reduced regulatory genes from our RT-PCR measurements, and two growth factor signaling molecules, *Fgf10* and *Wnt5a*, both known to function in postnatal lung development (Chao et al., 2016; Li et al., 2020a; Zhang et al., 2020). Secretome-receptome computation using the Fantom algorithm (Ramilowski et al., 2015) revealed the cognate receptors, FGFR1/3/4 and ROR2, involve in FGF10 and WNT5a signaling transduction within SCMF (Fig.4B). To investigate the possibility of cross regulation of these genes on the other altered SCMF genes, GFP⁺ SCMFs were isolated by FACS from postnatal *Gcre;mTmG* lungs and cultured in vitro (Fig.4 A). Cultures were treated with inhibitors that target the gene or pathway of interest. The inhibitor's dose was determined from the literature and a series of testing (Supplemental Table 2), and inhibition was validated by examining its target genes (SFig.4A). Blocking IGF1 signaling using IGF1R inhibitor (PPP at 4uM as in Chen et al., 2017; Jin et al., 2018; Wang et al., 2019), led to altered expression of all genes, except *Gli1*, in the same direction as observed in vivo (SFig.4B) indicating that isolated cells in vitro recapitulate the observed in vivo findings. Expression level of *Gli1* was too low to be reliably detected in culture, likely due to absence of HH signaling which in vivo is provided exclusively by the lung epithelium.

The signaling of FGF10 and the expression of *Wnt5a* and *Foxd1* were blocked in culture with FGFR inhibitor (Infigratinib at 1uM as in Manchado et al., 2016; Nakamura et al., 2015; Wong et al., 2018), siWnt5a (at 20nM as in Nemoto et al., 2012; Sakisaka et al., 2015; Zhao et al., 2017) and siFoxd1(at 20nM as in Li et al., 2021; Nakayama et al., 2015; Wu et al., 2018) respectively, and their effects on other SCMF genes were quantified by RT-PCR (Fig.4C). Identified genes with significant change are designated as targets of the gene/pathway perturbed, and their connections are plotted on the network (Fig.4D).

The architecture of the new construct reveals the identity of 3 transcription factors FOXD1, TBX2, and SOX8 forming a presumed connection hub. They are targeted by all 3 signaling pathways within the network and with each other as demonstrated by FOXD1's regulation of *Tbx2* and *Sox8*, likely representing a core network subcircuit (Peter and Davidson, 2009) tasked to lockdown a regulatory state so that the signaling effect from the upstream can be stabilized.

Alveolar epithelial genes are affected through WNT5a and FGF10 signaling.

As mentioned above, both AT1 and AT2 cells were reduced in *Gcre;Igf1r-f/f* mutant lungs (Fig.2C). To identify any genetic alterations within these cells, we analyzed our FACS-sorted Tomato⁺ cells (Fig.3A), in which the lung epithelial cells reside, for the expression of a broad list

of known AT1/AT2 signature genes including their canonical markers and the ones identified by scRNAseq (i.e. Treutlein et al., 2014; Nabhan et al., 2018; LungMap). The comparison between the control and the mutant data identified the genes significantly altered (Fig.5A).

Since our *Gcre;Igf1r-f/f* mutant was a SCMF targeted deletion, these changes must be a secondary consequence of intercellular cross communication. Within the altered SCMF gene list there are a total of 3 ligands: *Wnt5a*, *Fgf10* and *Cyr61* (Fig.4D). CYR61 is more commonly recognized as a matricellular protein (Lau, 2011) rather than a classical growth factor such as FGF10 and WNT5A. Secretome-receptome analysis indicates that FGF10 and WNT5a from SCMF communicate with alveolar epithelial cells thru their cognate receptors, FGFR2 and ROR1 (Fig.4B).

The intercellular connections discovered above, plus the affected epithelial genes were also added to the network as shown in Fig.5B. Multiple evidence has shown that IGF1 signaling can promote lung epithelial growth and development (Ghosh et al., 2013; Narasaraaju et al., 2006; Wang et al., 2018b). Our work here reveals a nearly comprehensive look at the genetic pathway behind that.

WNT5a is required for alveolar formation as inferred by the IGF1 signaling GRN.

Our effort so far has led to the successful construction of the IGF1 signaling GRN during alveologenesis. The network offers a novel bird's-eye view of how the genes involved in IGF1 signaling are connected in the form of a molecular circuitry for alveologenesis and a mechanistic perception of how this circuitry is firstly turned on in SCMF for the function of these cells and then advance to the neighboring alveolar epithelial cells to influence their cellular behaviors.

Under this mechanistic view, the position where a gene is located on the architecture of the network and the connections it has with other genes manifest its role and impact on the network's operation and outcome, thus its specific biological function in the process of alveolar formation. The network makes it possible to assess and predict a gene's function before it is tested in vivo.

Mainly derived from our in vitro data, it was discovered WNT5a signaling on the current network is located immediately downstream of IGF1 and the signaling has connections with many IGF1 downstream genes (Fig.5B). This indicates *Wnt5a*'s feed-forward role on the transduction of IGF1 signaling and its biological effect. Indeed, when *Wnt5a* is inactivated in mice, the mutant lungs exhibit a BPD-like phenotype with arrested alveologenesis, similar to what is seen in the *Igf1r* mutant (Fig.6). Inversely, the in vivo perturbation data collected from this *Wnt5a* mutant mouse model can be used to further define the regulatory connections where *Wnt5a* is involved on the current *Igf1* GRN.

A GRN of similar components and wiring underlies human BPD.

The expression of the mouse IGF1 signaling GRN regulatory genes in SCMF was also examined in lung samples from postmortem human BPD samples. The regulatory genes, on the upper hierarchy of the network, determine the network's outcome. In comparison to non-BPD lungs, 9 of the 12 genes examined were altered, and 8 were altered in the same direction as they were defined in the mouse GRN (Fig.7). These findings indicate a genetic program of similar components and wiring underlying human BPD.

Discussion

With massive gene expression data available (e.g., the LungMAP database) in this postgenomic era, one pressing job is to identify the function of the specific genes, and particularly how they interact with one another (Przybyla and Gilbert, 2021). With gene regulatory network analysis as our targeted approach, we have constructed the IGF1 signaling GRN underlying alveologenesis using a mouse model of BPD.

The application of the GRN approach in the lung field is novel as it hasn't been previously reported. Although not all the genes on the network have been examined by perturbation and the links haven't been determined as direct or indirect, the regulatory connections running along the constructed GRN are already able to provide potential mechanistic explanation as to how the effect of IGF1 signaling is transduced from one gene to a constellation of its downstream genes and from one cell type to another. Indeed, blocking Wnt5a signaling is confirmed to produce a mouse BPD-like phenotype as inferred by the network. Signaling by Igf1, Fgf10 and Wnt5a have been long recognized to have roles in alveologenesis (i.e. Chao et al., 2016; He et al., 2021; Li et al., 2020a; Zhang et al., 2020). The present GRN reveals a full genetic program behind and the cross-talk among them. The fact that all these signaling pathways have connections on the specification and effector genes of both alveolar mesenchymal and epithelial cells provides a direct causal link between the signaling and alveolar development.

Alveologenesis is a teamwork of a larger signaling network involving several different cell types. Within the mesenchymal cell type only, it is known that blocking IGF1, WNT5a, PDGFA and TGFβ signaling leads to impairment in development of alveoli though with different severity (Gao et al., 2022; He et al., 2021; Li et al., 2020a; Li et al., 2019b; Zhang et al., 2020). The sum of these leads to the construction of the hierarchical regulatory connections of these pathways within SCMF (Fig.8). Once signaling pathways from alveolar epithelium, endothelium and immune cells are included, a much larger and more comprehensive signaling GRN behind alveologenesis is expected to emerge.

Clinically, etiology of BPD is multifactorial and predominantly extrinsic. From GRN perspective, BPD is a developmental disease when the signaling GRN for alveologenesis is derailed and disrupted by these extrinsic factors. This disruption may happen within different cell types, onto different signaling pathways, and upon different hierarchy of the network (Fig.8). From the network's structural view, the disruption at the higher hierarchy has greater manifestation thus leading to disease of higher severity. Tgfb signaling, atop the whole hierarchy of the signaling GRN on Fig.8, exhibits in its mouse model mutant the most severe BPD-like phenotype when compared to mutants from the other signaling pathways under it (Chao et al., 2017; Gao et al., 2022; He et al., 2021; Li et al., 2020a; Li et al., 2019b). Also, different signaling sitting at different hierarchy has different coverage (sum of genes under the signaling's control) on the network. If disruption occurred beyond a signaling's coverage, the treatment by targeting this signaling would be off target. Igf1 signaling is discovered as in the middle hierarchy of the constructed network (Fig.8). By targeting one such signaling and hoping to treat BPD in general will surely not always work.

Our GRN view on alveologenesis presents a transformative viewing of BPD and could potentially help in designing novel strategies to prevent and treat BPD. As for prevention, the GRN suggests a study centered on the network's periphery with focus to cut off the extrinsic factors and block their connections to the intrinsic alveologenesis GRN. For treatment, it is a study on the network

itself with focus to recover and rescue the signaling pathways that have been disheveled. All this work calls for at the first place the construction of the whole alveologenesis GRN which includes all major signaling pathways involved within and between each cell type and a network assembly of the hierarchal regulatory connections among them. Though the network construction is currently not experimentally accessible in human model, our work shows the alveologenesis GRN is well conserved between mouse and human lungs. With the mouse model, the whole signaling GRN behind alveologenesis can be decoded as exemplified by our work here in this paper, and the impact of extrinsic factors/signaling pathways and their manipulation on the network can be modeled and tested. The insights collected can then be used to guide health delivery for BPD clinically. In general, patient's clinical exam and test are used to determine the extrinsic factors; cell type gene expression data from bronchoalveolar lavage and/or biopsy are used to reveal genes altered within alveolar compartment in patient's lung; implied extrinsic factors and altered genes are mapped onto the alveologenesis GRN where the disruptions can thus be defined; therapies proven to be successful from mouse modeling data can then be pursued to recover/rescue these breaking points clinically in the patient.

A web resource of the network and the data presented in this paper is made available to the public: <https://sites.google.com/view/the-alveologenesis-grn/home>, which we hope can be used as portal to promote any further studies and collaborations in this direction. GRN is traditionally a network built on chemical interactions (RNA, DNA, protein and other chemicals). It has been recognized these interactions can also happen at mechanical and electrical level (i.e. Azeloglu and Iyengar, 2015). Mechanosignaling is of particular interest in lung as the organ itself is born to function through its non-stopping mechanical movement. New technologies, including whole genome CRISPR perturbation and screening, epigenomic profiling, high resolution ChIP-seq, spatial genomics and cis-regulatory analysis, are sprouting with their potential use for a high throughput GRN construction (i.e. Cusanovich et al., 2018; Eng et al., 2019; Sanson et al., 2018; Skene and Henikoff, 2015). Our journey to decode the alveologenesis GRN is also an adventure to construct new version of GRNs with rising technologies.

MATERIALS AND METHODS

1. Mouse Breeding and Genotyping

All animal studies were conducted strictly according to protocols approved by the USC Institutional Animal Care and Use Committee (IACUC) (Los Angeles, CA, USA). The mice were housed and maintained in pathogen-free conditions at constant room temperature (20–22 °C), with a 12 h light/dark cycle, and free access to water and food. *Dermo1-cre*, *Gli1-cre^{ERT2}*, *Rosa26^{mTmG}*, *CAG^{tdTomato}*, *Igfl^(flox/flox)*, *Igflr^(flox/flox)*, *CAG-cre^{ER}*, and *Wnt5a^(flox/flox)* mice were purchased from the Jackson Laboratory. *Foxd1GCE* mouse were generated by McMahon lab at USC. *SPC^{GFP}* mice were generated by Wright lab at Duke University.

Dermo1-cre;Igfl^(flox/flox) (*Dcre;Igfl-f/f*) and *Dermo1-cre;Igflr^(flox/flox)* (*Dcre;Igflr-f/f*) mice were generated by breeding *Dermo1-cre* with *Igfl^(flox/flox)* and *Igflr^(flox/flox)* respectively.

Gli1-cre^{ERT2};Rosa26^{mTmG} mice were generated by breeding *Gli1-cre^{ERT2}* and *Rosa26^{mTmG}* mice.

Gli1-cre^{ERT2};Igflr^(flox/flox) (*Gcre;Igflr-f/f*) mice were generated by breeding *Gli1-cre^{ERT2}* mice with the *Igflr^(flox/flox)* mice.

Rosa26^{mTmG};Igflr^(flox/flox) (*mTmG;Igflr-f/f*) mice were generated by breeding *Rosa26^{mTmG}* mice with the *Igflr^(flox/flox)* mice.

Gli1-cre^{ERT2};Rosa26^{mTmG};Igflr^(flox/flox) (*Gcre;mTmG;Igflr-f/f*) mice were generated by breeding *Gli1-cre^{ERT2};Igflr^(flox/flox)* mice with the *Rosa26^{mTmG};Igflr^(flox/flox)* mice.

Foxd1GCE;CAG^{tdTomato} (*Fcre;Tomato*) mice were generated by breeding *Foxd1GCE* mice with the *CAG^{tdTomato}* mice.

CAG-cre^{ER};Wnt5a^(flox/flox) (*Ccre;Wnt5a-f/f*) mice were generated by breeding *CAG-cre^{ER}* mice with the *Wnt5a^(flox/flox)* mice.

Genotyping of the transgenic mice was performed by PCR with genomic DNA isolated from mouse tails. The forward (F) and reverse primers (R) for transgenic mouse genotyping are listed in Supplemental Table 3.

2. Tamoxifen Administration

A single dose of Tamoxifen (8mg/mL in peanut oil) was administered by oral gavage to neonates at postnatal day 2 (PN2, 400µg each pup) with a plastic feeding needle (Instech Laboratories, PA). Neonatal lungs were collected between PN7 and PN30 for morphological, immunohistochemical, cellular and molecular biological analyses.

3. Mouse lung tissue

Mice were euthanized by CO2 inhalation at the time of tissue harvest. Chest cavity was exposed and lungs cleared of blood by perfusion with cold PBS via the right ventricle. Lungs were inflated with 4% formaldehyde under constant 30cm H2O pressure and allowed to fix overnight at 4°C. Tissue was dehydrated through a series of ethanol washes after which they were embedded in paraffin and sectioned.

4. Immunohistochemistry

H&E staining was performed as usual, and morphometric measurements were made using ImageJ. Immunofluorescent staining was performed as previously described using paraffin-

embedded lung sections (Li et al., 2019a). In brief, five micrometer (μm) tissue sections were deparaffinized, rehydrated and subjected to antigen retrieval. After blocking with normal serum, the sections were probed with primary antibodies at 4°C overnight. Combinations of Alexa Fluor Plus secondary antibodies (Thermo Fisher Scientific) were applied for fluorescent detection of above specific primary antibodies. Nuclei were counterstained with 4',6-diamidino-2-phenylindole (DAPI). Primary antibodies used and their sources are listed in the Key Resources Table below. Images were made with Leica DMI8 fluorescence microscope and processed with Leica LAS X and ImageJ.

5. RNAScope

Samples were fixed in 10% neutral buffered formalin, dehydrated with ethanol and embedded in paraffin wax. $5\mu\text{m}$ Sections from paraffin blocks were processed using standard pretreatment conditions per the RNAScope multiplex fluorescent reagent kit version 2 (Advanced Cell Diagnostics) assay protocol. TSA-plus fluorescein, Cy3 and Cy5 fluorophores were used at different dilution optimized for each probe. RNAScope probes used are listed in the Key Resources Table below. Images were made with Leica DMI8 fluorescence microscope and processed with Leica LAS X and ImageJ.

6. Mouse lung single-cell dissociation

Single-cell suspension was prepared as described in Adam et al. (2017) with all the procedures performed on ice or in cold room. Mice were euthanized and the lungs were perfused with PBS as described above. The lungs were inflated with cold active protease solution (5mM CaCl_2 , 10 mg/ml *Bacillus Licheniformis* protease), dissected and transferred to a petri dish, and the heart, thymus and trachea were removed. The lobes were minced using a razor blade. The minced tissue was then immersed in extra cold active protease solution for 10 min and triturated using a 1ml pipet. This Homogenate was transferred to a Miltenyi C-tube with 5ml HBSS/DNase (Hank's Balanced Salt Buffer) and the Miltenyi gentleMACS lung program was run twice on GentleMACs Dissociator. Subsequently, this suspension was passed through a 100um strainer, pelleted at 300g for 6 minutes, suspended in 2ml RBC (Red Blood Cell) Lysis Buffer (BioLegend) and incubated for 2 min. At this point, 8ml HBSS was added and centrifuged again. The pellet was suspended in HBSS, then filtered through a 30um strainer. The suspension was pelleted again and finally suspended in MACS separation buffer (Miltenyi Biotec) with 2% FBS for Fluorescence-activated cell sorting (FACS). Cell separation and viability were examined under the microscope and through Vi-CELL Cell Counter after staining with Trypan blue.

7. Flow Cytometry and Cell Sorting

FACS was performed on a BD FACS Aria II at stem cell Flow Cytometry Core at Keck school of medicine USC. The sorting was gated on viability, singlets, GFP and/or Tomato. GFP+ and/or Tomato+ cells were collected as needed. For cell culture, cells were sorted in DMEM containing 10% FBS. For RNA, cells of interest were collected in Trizol-LS reagent (ThermoFisher).

8. RNA-seq analyses

Lungs dissected from *Sftpc*^{GFP} mouse at PN14 were dissociated into single cell suspension and GFP+ cells were sorted and collected as described above. RNA was extracted using Qiagen RNeasy Micro kit and then submitted to the Millard and Muriel Jacobs Genetics and Genomics Laboratory at Caltech for sequencing, which was run at 50bp, single end, and 30 million reading depth. The unaligned raw reads from aforementioned sequencing were processed on the

PartekFlow platform. In brief, read alignment, and gene annotation and quantification, were based on mouse genome (mm10) and transcriptome (GENECODE genes-release 7). Tophat2 and Upper Quartile algorithms were used for mapping and normalization. The RNA-seq data have been deposited with GEO under the accession number GSE182886.

9. Neonatal lung myofibroblast culture and treatment

FACS sorted GFP+ cells from PN5 neonatal lungs of *Gli1-cre^{ERT2};Rosa26^{mTmG}* mice were suspended in DMEM containing 10% FBS, plated in 24-well culture plates at 50,000 cells/well and incubated at 37°C with 5% CO₂ on day 1 after sorting. On day 2 after sorting, the attached myofibroblasts were washed with PBS and cultured in fresh medium with inhibitors or siRNAs as indicated in each experiment. The ON TARGETplus SMARTpool siRNAs from Dharmacon were used, and the transfection was done using DharmaFECT™ Transfection Reagents. On day 4, the cells were collected for RNA analyses. The cells were authenticated for absence of contaminations.

10. Real-time Quantitative Polymerase Chain Reaction (real-time RT-PCR)

Neonatal mouse lung cells were collected from FACS or cell culture as described above. The RNA was isolated with Direct-zol™ RNA MiniPrep kit according to the manufacturer's protocol (ZYMO Research). Following RNA purification, cDNA was generated using the SuperScript IV First-Strand Synthesis System (ThermoFisher). Expression of selected genes was quantified by Quantitative Real Time RT-PCR performed on a Light Cycler (Roche) or 7900HT fast real-time PCR system (Applied Biosystems) using SYBR green reagents (ThermoFisher). The deltaCT method was used to calculate relative ratios of a target gene mRNA in mutant lungs compared to littermate control lungs. *Gapdh* was used as the reference gene. Primers for each gene were designed on IDT website and the specificity of their amplification was verified by their melting curve. Sequences of the primers are listed in Supplemental Table 3.

11. Human neonatal lung samples

BPD and non-BPD postnatal human lung tissues were provided by the International Institute for the Advancement of Medicine and the National Disease Research Interchange, and were classified exempt from human subject regulations per the University of Rochester Research Subjects Review Board protocol (RSRB00056775).

12. Bioinformatic Methods

Cell to cell communications were predicted using a published Fantom5 Cell Connectome dataset linking ligands to their receptors (STAR Methods) (Ramilowski et al., 2015).

The ligands and receptors were identified from the following RNAseq dataset with GLI1+ cells for SCMF (accession#: GSE126457 from Li et al., 2019a), SFTPC+ cells for AT2 (accession#: GSE182886) and PDPN+ cells for AT1 (accession#: GSE106960 from Wang et al., 2018a).

The IGF1 signaling GRN was drawn in BioTapestry software developed by Longabaugh et al. (2012).

13. Statistical Analysis

At least three biological replicates for each experimental group were used for quantification and comparative analysis. At least 10 images (10x magnification) from each lung were used for morphometric quantification. Statistical analysis was performed in JMP pro 15. A two-tailed

Student's T-Test was used for the comparison between two experimental groups and a one-way ANOVA was used for multiple comparisons. Quantitative data are presented as mean values +/- SD. Data were considered significant if $p < 0.05$.

KEY RESOURCES TABLE

Reagent or Resource	Source	Identifier	Working Concentration
Antibodies			
ACTA2	Abcam	Cat#: AB5694	1:300
ACTC1	Santa Cruz	Cat#: SC-58670	1:100
ADRP	Abcam	Cat#: AB108323	1:200
AQP5	Alomone	Cat#: AQP-005	1:100
BMPER	Santa Cruz	Cat#: SC-377502	1:200
CAS3	Cell Signaling	Cat#: 9664	1:100
ELN	Abcam	Cat#: AB21600	1:200
EMCN	R&D Systems	Cat#: AF4666	1:100
GFP	Santa Cruz	Cat#: SC-9996	1:100
HOPX	Santa Cruz	Cat#: SC-30216	1:50
KI67	R&D Systems	Cat#: AF7649	1:50
NKX2.1	Seven Hills	Cat#: 8G7G3-1	1:50
NG2	Abcam	Cat#: AB5320	1:100
PDGFRa	Cell Signaling	Cat#: 3174	1:50
PDPN	Thermo Fisher	Cat#: 14-5381-82	1:300
RFP	Rockland	Cat#: 600-401-379S	1:300
SFTPC	Abcam	Cat#: AB3786	1:200
SOX8	Santa Cruz	Cat#: SC-374446	1:50
TBX2	Santa Cruz	Cat#: SC-514291	1:50
TPM1	Sigma Aldrich	Cat#: T2780	1:500
Chemicals and Inhibitors			
Tamoxifen	Sigma	Cat#: T5648	8mg/ml

Infigratinib	Selleckchem	Cat#: S2788	1uM
PPP	Selleckchem	Cat#: S7668	4uM
siFoxd1	Dharmacon	Cat#: L-046204-00-0005	20nM
siWnt5a	Dharmacon	Cat#: L-065584-01-0005	20nM
siRNA non-targeting	Dharmacon	Cat#: D-001810-01-05	20nM

Sequencing

Next Ultra DNA Library Prep Kit	New England Biolabs	Cat#: E7370	
Bulk RNAseq	Millard and Muriel Jacobs Genetics and Genomics Laboratory at Caltech	GEO: GSE182886	

Mouse

<i>Gli1-cre^{ERT2}</i>	Jackson Laboratories	Cat#: 007913	
<i>Rosa26^{mTmG}</i>	Jackson Laboratories	Cat#: 007676	
<i>CAG^{Tomato}</i>	Jackson Laboratories	Cat#: 007914	
<i>Dermo1-cre</i>	Jackson Laboratories	Cat#: 028701	
<i>Igf1^(flox/flox)</i>	Jackson Laboratories	Cat#: 016831	
<i>Igf1r^(flox/flox)</i>	Jackson Laboratories	Cat#: 012251	
<i>CAG-cre^{ER}</i>	Jackson Laboratories	Cat#: 004453	
<i>Wnt5a^(flox/flox)</i>	Jackson Laboratories	Cat#: 026626	
<i>Foxd1GCE</i>	McMahon Laboratory		

RNA Scope

RNA scope® Multiplex Fluorescent Reagent Kit V2	Advanced Cell Diagnostics	Cat#: 323100	
<i>Igf1</i>	Advanced Cell Diagnostics	Cat#: 443901-C1	1:750
<i>Igf1r</i>	Advanced Cell Diagnostics	Cat#: 417561-C3	1:500
<i>Pdgfra</i>	Advanced Cell Diagnostics	Cat#: 480661-C2	1:750
<i>Fgf10</i>	Advanced Cell Diagnostics	Cat#: 446371-C1	1:750

<i>Wnt5a</i>	Advanced Cell Diagnostics	Cat#: 316791-C3	1:500
RNAscope® 3-plex Positive Control Probe Mm	Advanced Cell Diagnostics	Cat#: 320881	1:1500
RNAscope® 3-plex Negative Control Probe	Advanced Cell Diagnostics	Cat#: 320871	1:1500

Software and Algorithms

Image J	NIH	https://imagej.nih.gov/ij/
STAR 2.5	PMCID: PMC3530905	https://github.com/alexdobin/STAR
JMP pro 15	Statistical Discovery	https://www.jmp.com/en_us/software/predictive-analytics-software.html
Fantom5 Cell Connectome	FANTOM5 project	https://fantom.gsc.riken.jp/5/suppl/Ramilowski_et_al_2015/vis/#/hive
Imaris	BitPlane	http://www.bitplane.com/imaris/imaris
R 3.2	R Project	https://www.r-project.org/
LAS X	Leica	https://www.leica-microsystems.com/products/microscope-software/p/leica-las-x-ls/
BioTapestry	Institute for Systems Biology	http://www.biotapestry.org/

1

2

3

4

5

Acknowledgements: We thank Dr. Andrew P. McMahon (Keck School of Medicine of USC) for providing the *Foxd1*^{GCE;CAG^{tdTomato} mice. We thank Arnold Sipos (Keck School of Medicine of USC) for help with imaging and Sean Gao (Arcadia High School) for data analysis and the construction of alveologenesis GRN website.}

Competing Interests: No.

Fundings: This work was supported by the National Institutes of Health [HL144932, HL122764 (C.L. & P.M.), HL143059 (P.M.), R35 HL135747 (Z.B. & P.M.)], the Hastings Foundation (P.M., Z.B.).

Author Contributions: Conceptualization: F.G., C.L., P.M.; Data curation: F.G., C.L., P.M.; Investigation: F.G., C.L., S.M.S., N.P., G.K., E.T., E.L., W.L.; Methodology: F.G., C.L., P.M.; Validation: F.G., C.L., P.M.; Project administration: C.L., P.M.; Funding acquisition: C.L., P.M.; Writing – original draft: F.G., P.M.; Writing – review & editing: F.G., P.M., C.L., E.T., B.Z.

Data Availability Statement: Additional data that support the findings of this study are available on request from the corresponding author.

REFERENCES

- Adam, M., Potter, A.S., Potter, S.S., 2017. Psychrophilic proteases dramatically reduce single-cell RNA-seq artifacts: a molecular atlas of kidney development. *Development* 144, 3625-3632.
- Azeloglu, E.U., Iyengar, R., 2015. Signaling networks: information flow, computation, and decision making. *Cold Spring Harb Perspect Biol* 7, a005934.
- Barber, R.D., Harmer, D.W., Coleman, R.A., Clark, B.J., 2005. GAPDH as a housekeeping gene: analysis of GAPDH mRNA expression in a panel of 72 human tissues. *Physiol Genomics* 21, 389-395.
- Branchfield, K., Li, R., Lungova, V., Verheyden, J.M., McCulley, D., Sun, X., 2016. A three-dimensional study of alveologenesis in mouse lung. *Developmental Biology* 409, 429-441.
- Carre, C., Mas, A., Krouk, G., 2017. Reverse engineering highlights potential principles of large gene regulatory network design and learning. *NPJ Syst Biol Appl* 3, 17.
- Chao, C.M., Moiseenko, A., Zimmer, K.P., Bellusci, S., 2016. Alveologenesis: key cellular players and fibroblast growth factor 10 signaling. *Mol Cell Pediatr* 3, 17.
- Chao, C.M., Yahya, F., Moiseenko, A., Tiozzo, C., Shrestha, A., Ahmadvand, N., El Agha, E., Quantius, J., Dilai, S., Kheirollahi, V., Jones, M., Wilhem, J., Carraro, G., Ehrhardt, H., Zimmer, K.P., Barreto, G., Ahlbrecht, K., Morty, R.E., Herold, S., Abellar, R.G., Seeger, W., Schermuly, R., Zhang, J.S., Minoo, P., Bellusci, S., 2017. Fgf10 deficiency is causative for lethality in a mouse model of bronchopulmonary dysplasia. *J Pathol* 241, 91-103.
- Chen, L., Chen, Q., Rong, P., Wang, H.Y., Chen, S., 2017. The energy sensing LKB1-AMPKalpha1 pathway regulates IGF1 secretion and consequent activation of the IGF1R-PKB pathway in primary hepatocytes. *FEBS J* 284, 2096-2109.
- Cusanovich, D.A., Hill, A.J., Aghamirzaie, D., Daza, R.M., Pliner, H.A., Berletch, J.B., Filippova, G.N., Huang, X., Christiansen, L., DeWitt, W.S., Lee, C., Regalado, S.G., Read, D.F., Steemers, F.J., Disteche, C.M., Trapnell, C., Shendure, J., 2018. A Single-Cell Atlas of In Vivo Mammalian Chromatin Accessibility. *Cell* 174, 1309-1324 e1318.
- Davidson, E.H., 2010. Emerging properties of animal gene regulatory networks. *Nature* 468, 911-920.
- Davidson, E.H., Rast, J.P., Oliveri, P., Ransick, A., Caestani, C., Yuh, C.H., Minokawa, T., Amore, G., Hinman, V., Arenas-Mena, C., Otim, O., Brown, C.T., Livi, C.B., Lee, P.Y., Revilla, R., Rust, A.G., Pan, Z., Schilstra, M.J., Clarke, P.J., Arnone, M.I., Rowen, L., Cameron, R.A., McClay, D.R., Hood, L., Bolouri, H., 2002. A genomic regulatory network for development. *Science* 295, 1669-1678.
- Dequeant, M.L., Pourquie, O., 2008. Segmental patterning of the vertebrate embryonic axis. *Nat Rev Genet* 9, 370-382.
- Eng, C.L., Lawson, M., Zhu, Q., Dries, R., Koulana, N., Takei, Y., Yun, J., Cronin, C., Karp, C., Yuan, G.C., Cai, L., 2019. Transcriptome-scale super-resolved imaging in tissues by RNA seqFISH. *Nature* 568, 235-239.
- Epaud, R., Aubey, F., Xu, J., Chaker, Z., Clemessy, M., Dautin, A., Ahamed, K., Bonora, M., Hoyeau, N., Flejou, J.F., Mailleux, A., Clement, A., Henrion-Caude, A., Holzenberger, M., 2012. Knockout of insulin-like growth factor-1 receptor impairs distal lung morphogenesis. *PloS one* 7, e48071.

- 1 Erwin, D.H., Davidson, E.H., 2009. The evolution of hierarchical gene regulatory networks. *Nat*
2 *Rev Genet* 10, 141-148.
- 3 Gao, F., Davidson, E.H., 2008. Transfer of a large gene regulatory apparatus to a new
4 developmental address in echinoid evolution. *Proceedings of the National Academy of Sciences*
5 *of the United States of America* 105, 6091-6096.
- 6 Gao, F., Li, C., Danopoulos, S., Al Alam, D., Peinado, N., Webster, S., Borok, Z., Kohbodi,
7 A.G., Bellusci, S., Minoo, P., 2022. Hedgehog-Responsive PDGFRa(+) Fibroblasts are
8 Necessary for Maintenance of a Unique Pool of Alveolar Epithelial Progenitor Cells During
9 Alveologenesis. *Cell Rep*, In Press.
- 10 Ghosh, M.C., Gorantla, V., Makena, P.S., Luellen, C., Sinclair, S.E., Schwingshackl, A., Waters,
11 C.M., 2013. Insulin-like growth factor-I stimulates differentiation of ATII cells to ATI-like cells
12 through activation of Wnt5a. *Am J Physiol Lung Cell Mol Physiol* 305, L222-228.
- 13 He, H., Snowball, J., Sun, F., Na, C.L., Whitsett, J.A., 2021. IGF1R controls mechanosignaling
14 in myofibroblasts required for pulmonary alveologenesis. *JCI Insight* 6.
- 15 Jain, D., Bancalari, E., 2014. Bronchopulmonary dysplasia: clinical perspective. *Birth Defects*
16 *Res A Clin Mol Teratol* 100, 134-144.
- 17 Jia, B., Xu, S., Xiao, G., Lamba, V., Liang, F., 2017. Learning gene regulatory networks from
18 next generation sequencing data. *Biometrics* 73, 1221-1230.
- 19 Jin, K., Ruan, L., Pu, J., Zhong, A., Wang, F., Tan, S., Huang, H., Mu, J., Yang, G., 2018.
20 Metformin suppresses growth and adrenocorticotrophic hormone secretion in mouse pituitary
21 corticotroph tumor AtT20cells. *Mol Cell Endocrinol* 478, 53-61.
- 22 Jobe, A.J., 1999. The new BPD: an arrest of lung development. *Pediatr Res* 46, 641-643.
- 23 Juul, N.H., Stockman, C.A., Desai, T.J., 2020. Niche Cells and Signals that Regulate Lung
24 Alveolar Stem Cells In Vivo. *Cold Spring Harb Perspect Biol* 12.
- 25 Lau, L.F., 2011. CCN1/CYR61: the very model of a modern matricellular protein. *Cell Mol Life*
26 *Sci* 68, 3149-3163.
- 27 Levine, M., Davidson, E.H., 2005. Gene regulatory networks for development. *Proc Natl Acad*
28 *Sci U S A* 102, 4936-4942.
- 29 Ley, D., Hallberg, B., Hansen-Pupp, I., Dani, C., Ramenghi, L.A., Marlow, N., Beardsall, K.,
30 Bhatti, F., Dunger, D., Higginson, J.D., Mahaveer, A., Mezu-Ndubuisi, O.J., Reynolds, P.,
31 Giannantonio, C., van Weissenbruch, M., Barton, N., Tocoian, A., Hamdani, M., Jochim, E.,
32 Mangili, A., Chung, J.K., Turner, M.A., Smith, L.E.H., Hellstrom, A., study, t., 2019. rhIGF-
33 1/rhIGFBP-3 in Preterm Infants: A Phase 2 Randomized Controlled Trial. *J Pediatr* 206, 56-65
34 e58.
- 35 Li, C., Lee, M.K., Gao, F., Webster, S., Di, H., Duan, J., Yang, C.Y., Bhopal, N., Peinado, N.,
36 Pryhuber, G., Smith, S.M., Borok, Z., Bellusci, S., Minoo, P., 2019a. Secondary crest
37 myofibroblast PDGFRalpha controls the elastogenesis pathway via a secondary tier of signaling
38 networks during alveologenesis. *Development* 146.
- 39 Li, C., Li, M., Li, S., Xing, Y., Yang, C.Y., Li, A., Borok, Z., De Langhe, S., Minoo, P., 2015.
40 Progenitors of secondary crest myofibroblasts are developmentally committed in early lung
41 mesoderm. *Stem Cells* 33, 999-1012.

- 1 Li, C., Smith, S.M., Peinado, N., Gao, F., Li, W., Lee, M.K., Zhou, B., Bellusci, S., Pryhuber,
2 G.S., Ho, H.H., Borok, Z., Minoo, P., 2020a. WNT5a-ROR Signaling Is Essential for
3 Alveologenesis. *Cells* 9.
- 4 Li, C.G., Lee, M.K., Gao, F., Webster, S., Di, H.L., Duan, J., Yang, C.Y., Bhopal, N., Peinado,
5 N., Pryhuber, G., Smith, S.M., Borok, Z., Bellusci, S., Minoo, P., 2019b. Secondary crest
6 myofibroblast PDGFR alpha controls the elastogenesis pathway via a secondary tier of signaling
7 networks during alveologenesis. *Development* 146.
- 8 Li, J., Yan, T., Wu, X., Ke, X., Li, X., Zhu, Y., Yang, J., Li, Z., 2021. Aberrant overexpression
9 of transcription factor Forkhead box D1 predicts poor prognosis and promotes cancer
10 progression in HNSCC. *BMC Cancer* 21, 1205.
- 11 Li, M., Li, C., Liu, Y.H., Xing, Y., Hu, L., Borok, Z., Kwong, K.Y., Minoo, P., 2008.
12 Mesodermal deletion of transforming growth factor-beta receptor II disrupts lung epithelial
13 morphogenesis: cross-talk between TGF-beta and Sonic hedgehog pathways. *J Biol Chem* 283,
14 36257-36264.
- 15 Li, R., Bernau, K., Sandbo, N., Gu, J., Preissl, S., Sun, X., 2018. Pdgfra marks a cellular lineage
16 with distinct contributions to myofibroblasts in lung maturation and injury response. *Elife* 7.
- 17 Li, R., Li, X., Hagood, J., Zhu, M.S., Sun, X., 2020b. Myofibroblast contraction is essential for
18 generating and regenerating the gas-exchange surface. *J Clin Invest* 130, 2859-2871.
- 19 Lim, W.A., Lee, C.M., Tang, C., 2013. Design principles of regulatory networks: searching for
20 the molecular algorithms of the cell. *Mol Cell* 49, 202-212.
- 21 Longabaugh, W.J., 2012. BioTapestry: a tool to visualize the dynamic properties of gene
22 regulatory networks. *Methods Mol Biol* 786, 359-394.
- 23 Longabaugh, W.J.R., Zeng, W., Zhang, J.A., Hosokawa, H., Jansen, C.S., Li, L., Romero-Wolf,
24 M., Liu, P., Kueh, H.Y., Mortazavi, A., Rothenberg, E.V., 2017. Bcl11b and combinatorial
25 resolution of cell fate in the T-cell gene regulatory network. *Proc Natl Acad Sci U S A* 114,
26 5800-5807.
- 27 Lopez, I.P., Pineiro-Hermida, S., Pais, R.S., Torrens, R., Hoeflich, A., Pichel, J.G., 2016.
28 Involvement of Igflr in Bronchiolar Epithelial Regeneration: Role during Repair Kinetics after
29 Selective Club Cell Ablation. *PloS one* 11, e0166388.
- 30 Lopez, I.P., Rodriguez-de la Rosa, L., Pais, R.S., Pineiro-Hermida, S., Torrens, R., Contreras, J.,
31 Varela-Nieto, I., Pichel, J.G., 2015. Differential organ phenotypes after postnatal Igflr gene
32 conditional deletion induced by tamoxifen in UBC-CreERT2; Igflr fl/fl double transgenic mice.
33 *Transgenic Res* 24, 279-294.
- 34 Machado, E., Weissmueller, S., Morris, J.P.t., Chen, C.C., Wullenkord, R., Lujambio, A., de
35 Stanchina, E., Poirier, J.T., Gainor, J.F., Corcoran, R.B., Engelman, J.A., Rudin, C.M., Rosen,
36 N., Lowe, S.W., 2016. A combinatorial strategy for treating KRAS-mutant lung cancer. *Nature*
37 534, 647-651.
- 38 Materna, S.C., Oliveri, P., 2008. A protocol for unraveling gene regulatory networks. *Nat Protoc*
39 3, 1876-1887.
- 40 Nabhan, A.N., Brownfield, D.G., Harbury, P.B., Krasnow, M.A., Desai, T.J., 2018. Single-cell
41 Wnt signaling niches maintain stemness of alveolar type 2 cells. *Science* 359, 1118-1123.

- 1 Nakamura, H., Arai, Y., Totoki, Y., Shiota, T., Elzawahry, A., Kato, M., Hama, N., Hosoda, F.,
2 Urushidate, T., Ohashi, S., Hiraoka, N., Ojima, H., Shimada, K., Okusaka, T., Kosuge, T.,
3 Miyagawa, S., Shibata, T., 2015. Genomic spectra of biliary tract cancer. *Nat Genet* 47, 1003-
4 1010.
- 5 Nakayama, S., Soejima, K., Yasuda, H., Yoda, S., Satomi, R., Ikemura, S., Terai, H., Sato, T.,
6 Yamaguchi, N., Hamamoto, J., Arai, D., Ishioka, K., Ohgino, K., Naoki, K., Betsuyaku, T.,
7 2015. FOXD1 expression is associated with poor prognosis in non-small cell lung cancer.
8 *Anticancer Res* 35, 261-268.
- 9 Narasaraaju, T.A., Chen, H., Weng, T., Bhaskaran, M., Jin, N., Chen, J., Chen, Z., Chinoy, M.R.,
10 Liu, L., 2006. Expression profile of IGF system during lung injury and recovery in rats exposed
11 to hyperoxia: a possible role of IGF-1 in alveolar epithelial cell proliferation and differentiation.
12 *J Cell Biochem* 97, 984-998.
- 13 Nemoto, E., Ebe, Y., Kanaya, S., Tsuchiya, M., Nakamura, T., Tamura, M., Shimauchi, H.,
14 2012. Wnt5a signaling is a substantial constituent in bone morphogenetic protein-2-mediated
15 osteoblastogenesis. *Biochem Biophys Res Commun* 422, 627-632.
- 16 Olson, E.N., 2006. Gene regulatory networks in the evolution and development of the heart.
17 *Science* 313, 1922-1927.
- 18 Peter, I.S., Davidson, E.H., 2009. Modularity and design principles in the sea urchin embryo
19 gene regulatory network. *FEBS Lett* 583, 3948-3958.
- 20 Peter, I.S., Davidson, E.H., 2017. Assessing regulatory information in developmental gene
21 regulatory networks. *Proc Natl Acad Sci U S A* 114, 5862-5869.
- 22 Peter, I.S., Faure, E., Davidson, E.H., 2012. Predictive computation of genomic logic processing
23 functions in embryonic development. *Proc Natl Acad Sci U S A* 109, 16434-16442.
- 24 Pires-daSilva, A., Sommer, R.J., 2003. The evolution of signalling pathways in animal
25 development. *Nat Rev Genet* 4, 39-49.
- 26 Przybyla, L., Gilbert, L.A., 2021. A new era in functional genomics screens. *Nat Rev Genet*.
- 27 Ramilowski, J.A., Goldberg, T., Harshbarger, J., Kloppmann, E., Lizio, M., Satagopam, V.P.,
28 Itoh, M., Kawaji, H., Carninci, P., Rost, B., Forrest, A.R., 2015. A draft network of ligand-
29 receptor-mediated multicellular signalling in human. *Nat Commun* 6, 7866.
- 30 Sakisaka, Y., Tsuchiya, M., Nakamura, T., Tamura, M., Shimauchi, H., Nemoto, E., 2015.
31 Wnt5a attenuates Wnt3a-induced alkaline phosphatase expression in dental follicle cells. *Exp*
32 *Cell Res* 336, 85-93.
- 33 Sanson, K.R., Hanna, R.E., Hegde, M., Donovan, K.F., Strand, C., Sullender, M.E., Vaimberg,
34 E.W., Goodale, A., Root, D.E., Piccioni, F., Doench, J.G., 2018. Optimized libraries for
35 CRISPR-Cas9 genetic screens with multiple modalities. *Nat Commun* 9, 5416.
- 36 Satou, Y., Satoh, N., Imai, K.S., 2009. Gene regulatory networks in the early ascidian embryo.
37 *Biochim Biophys Acta* 1789, 268-273.
- 38 Sauka-Spengler, T., Bronner-Fraser, M., 2008. A gene regulatory network orchestrates neural
39 crest formation. *Nat Rev Mol Cell Biol* 9, 557-568.
- 40 Seedorf, G., Kim, C., Wallace, B., Mandell, E.W., Nowlin, T., Shepherd, D., Abman, S.H., 2020.
41 rhIGF-1/BP3 Preserves Lung Growth and Prevents Pulmonary Hypertension in Experimental
42 Bronchopulmonary Dysplasia. *Am J Respir Crit Care Med* 201, 1120-1134.

- 1 Short, E.J., Kirchner, H.L., Asaad, G.R., Fulton, S.E., Lewis, B.A., Klein, N., Eisengart, S.,
2 Baley, J., Kerckmar, C., Min, M.O., Singer, L.T., 2007. Developmental sequelae in preterm
3 infants having a diagnosis of bronchopulmonary dysplasia: analysis using a severity-based
4 classification system. *Arch Pediatr Adolesc Med* 161, 1082-1087.
- 5 Skene, P.J., Henikoff, S., 2015. A simple method for generating high-resolution maps of
6 genome-wide protein binding. *Elife* 4, e09225.
- 7 Tsao, P.N., Matsuoka, C., Wei, S.C., Sato, A., Sato, S., Hasegawa, K., Chen, H.K., Ling, T.Y.,
8 Mori, M., Cardoso, W.V., Morimoto, M., 2016. Epithelial Notch signaling regulates lung
9 alveolar morphogenesis and airway epithelial integrity. *Proc Natl Acad Sci U S A* 113, 8242-
10 8247.
- 11 Verheyden, J.M., Sun, X., 2020. A transitional stem cell state in the lung. *Nat Cell Biol* 22,
12 1025-1026.
- 13 Wang, G., Yin, L., Peng, Y., Gao, Y., Gao, H., Zhang, J., Lv, N., Miao, Y., Lu, Z., 2019. Insulin
14 promotes invasion and migration of KRAS(G12D) mutant HPNE cells by upregulating MMP-2
15 gelatinolytic activity via ERK- and PI3K-dependent signalling. *Cell Prolif* 52, e12575.
- 16 Wang, Y., Tang, Z., Huang, H., Li, J., Wang, Z., Yu, Y., Zhang, C., Li, J., Dai, H., Wang, F.,
17 Cai, T., Tang, N., 2018a. Pulmonary alveolar type I cell population consists of two distinct
18 subtypes that differ in cell fate. *Proc Natl Acad Sci U S A* 115, 2407-2412.
- 19 Wang, Z., Li, W., Guo, Q., Wang, Y., Ma, L., Zhang, X., 2018b. Insulin-Like Growth Factor-1
20 Signaling in Lung Development and Inflammatory Lung Diseases. *Biomed Res Int* 2018,
21 6057589.
- 22 Wong, G.S., Zhou, J., Liu, J.B., Wu, Z., Xu, X., Li, T., Xu, D., Schumacher, S.E., Puschhof, J.,
23 McFarland, J., Zou, C., Dulak, A., Henderson, L., Xu, P., O'Day, E., Rendak, R., Liao, W.L.,
24 Cecchi, F., Hembrough, T., Schwartz, S., Szeto, C., Rustgi, A.K., Wong, K.K., Diehl, J.A.,
25 Jensen, K., Graziano, F., Ruzzo, A., Fereshetian, S., Mertins, P., Carr, S.A., Beroukhi, R.,
26 Nakamura, K., Oki, E., Watanabe, M., Baba, H., Imamura, Y., Catenacci, D., Bass, A.J., 2018.
27 Targeting wild-type KRAS-amplified gastroesophageal cancer through combined MEK and
28 SHP2 inhibition. *Nat Med* 24, 968-977.
- 29 Wu, H., Larribere, L., Sun, Q., Novak, D., Sachindra, S., Granados, K., Umansky, V., Utikal, J.,
30 2018. Loss of neural crest-associated gene FOXD1 impairs melanoma invasion and migration
31 via RAC1B downregulation. *Int J Cancer* 143, 2962-2972.
- 32 Wu, H., Tang, N., 2021. Stem cells in pulmonary alveolar regeneration. *Development* 148.
- 33 Xu, Y., Wang, Y., Besnard, V., Ikegami, M., Wert, S.E., Heffner, C., Murray, S.A., Donahue,
34 L.R., Whitsett, J.A., 2012. Transcriptional programs controlling perinatal lung maturation. *PloS*
35 *one* 7, e37046.
- 36 Zepp, J.A., Morrissey, E.E., 2019. Cellular crosstalk in the development and regeneration of the
37 respiratory system. *Nat Rev Mol Cell Biol* 20, 551-566.
- 38 Zhang, K., Yao, E., Lin, C., Chou, Y.T., Wong, J., Li, J., Wolters, P.J., Chuang, P.T., 2020. A
39 mammalian Wnt5a-Ror2-Vangl2 axis controls the cytoskeleton and confers cellular properties
40 required for alveologenesis. *Elife* 9.
- 41 Zhao, G., Cheng, X.W., Piao, L., Hu, L., Lei, Y., Yang, G., Inoue, A., Ogasawara, S., Wu, H.,
42 Hao, C.N., Okumura, K., Kuzuya, M., 2017. The Soluble VEGF Receptor sFlt-1 Contributes to
43 Impaired Neovascularization in Aged Mice. *Aging Dis* 8, 287-300.

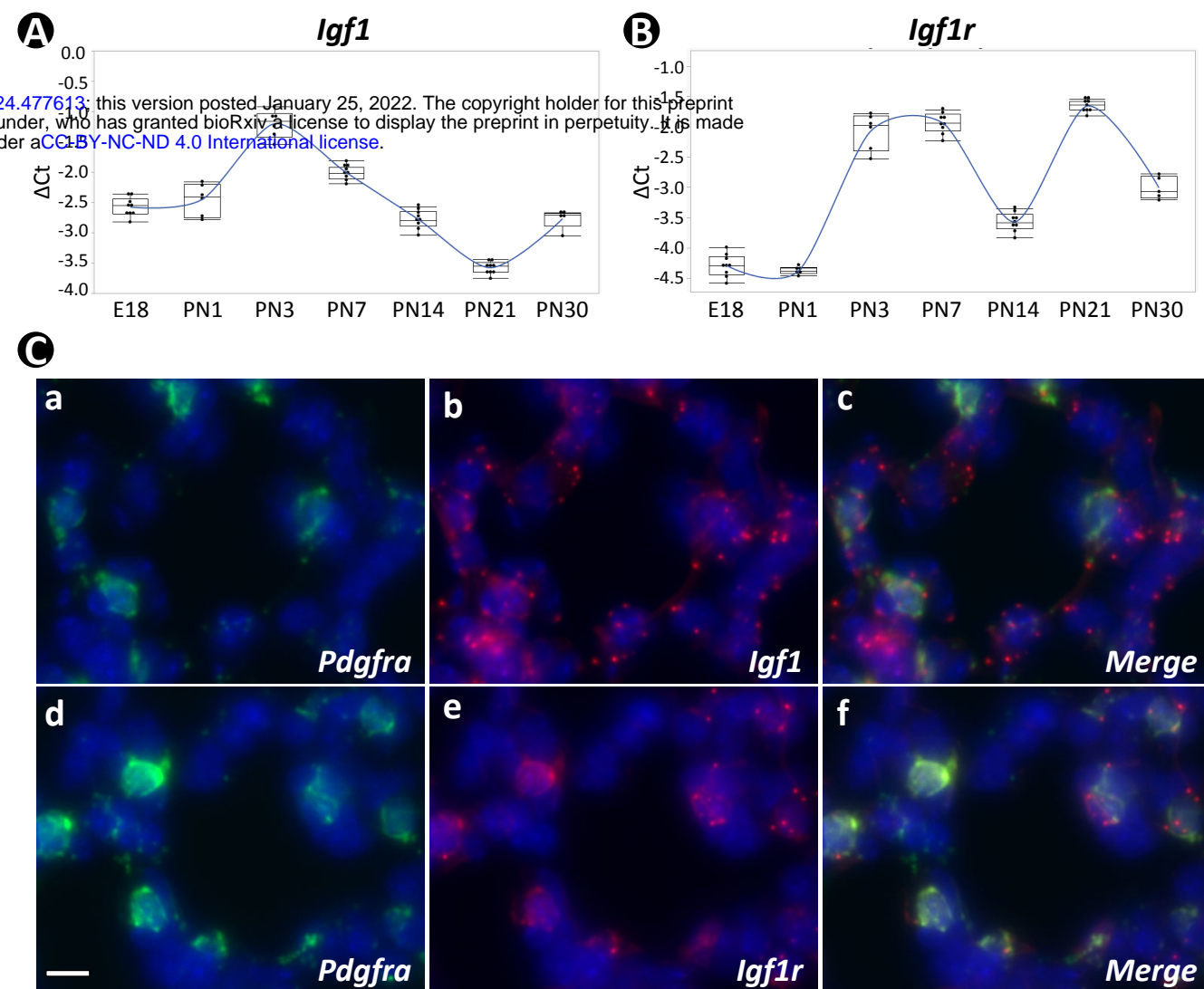


Figure 1: Temporal and spatial expression of *Igf1* and *Igf1r* during neonatal lung development in mouse. A, B: Temporal expression of *Igf1* (A) and *Igf1r* (B) from E18 to PN30, quantified by RT-PCR and normalized to *Gapdh*. C: Spatial localization of mRNA for *Igf1* (a-c) and *Igf1r* (d-f) in PN7 lungs as detected by RNAscope and their overlapped expression with *Pdgfra*. Scale bar: 10um for all images.

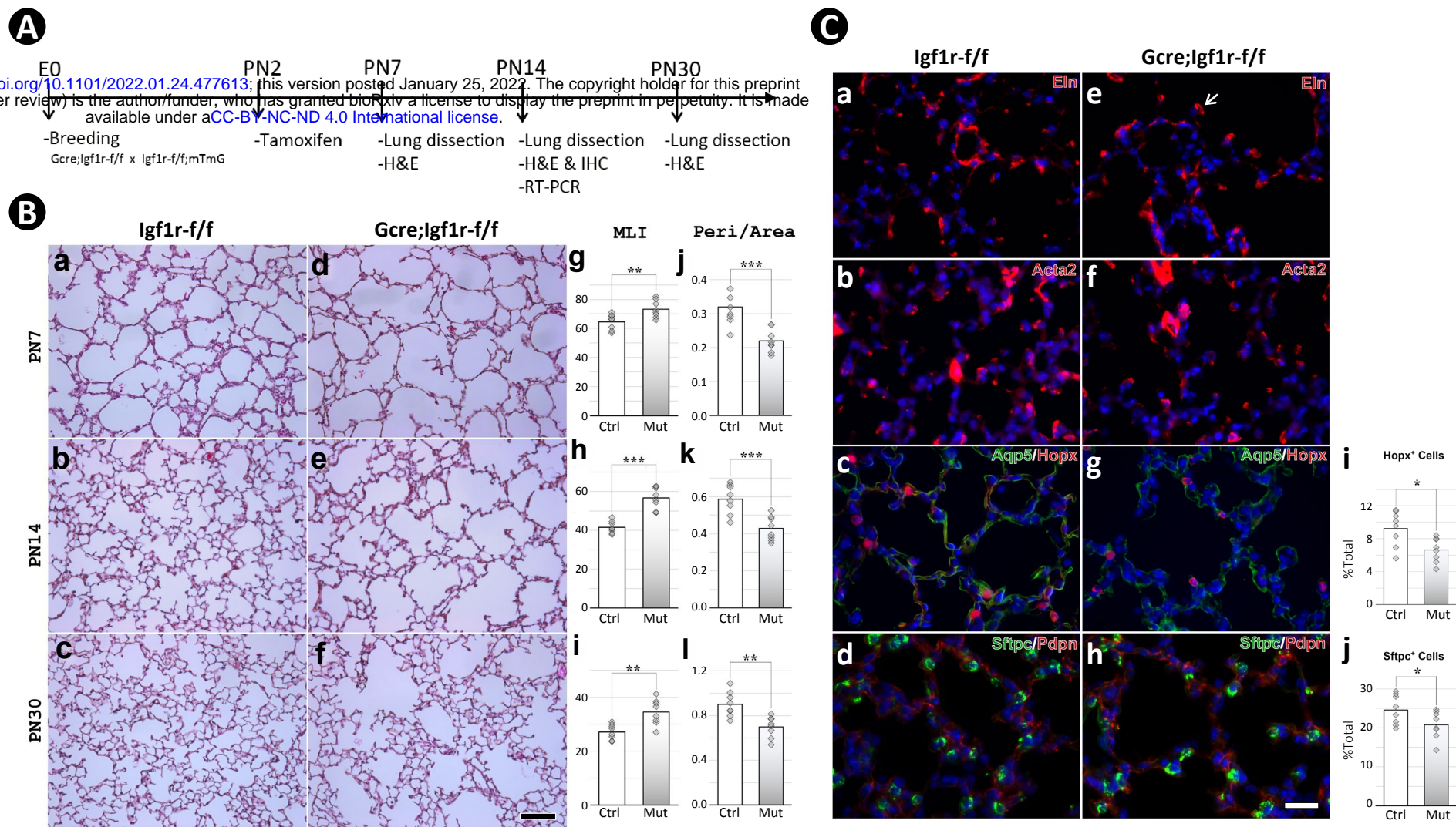


Figure 2: Postnatal inactivation of Igf1r from lung secondary crest myofibroblast cells. A: Schematic of the experimental protocol. B: H&E staining of lung sections from control (a-c) and *Gli1-cre^{ERT2}* mutant (d-f) mice and their morphometric measurements by MLI (g-i) and Peri/Area ratio (j-l) at PN7, PN14 and PN30. See Supplemental Figure 2 for the definition and calculation of these indices. C: Immunostaining of lung sections from control (a-d) and mutant (e-h) mice for Elastin (a,e), ACTA2 (b,f), AQP5/HOPX (c,g) and SFTPC/PDPN (d,h), and the comparison of number of AT1 (i) and AT2 (j) cells between control and mutant. Scale bar: 100um in B and 25um in C. *p*-value: * stands for 0.05-0.001, ** for 0.01-0.001, *** for <0.001, n.s. for not significant, and the same designation is used through the paper.

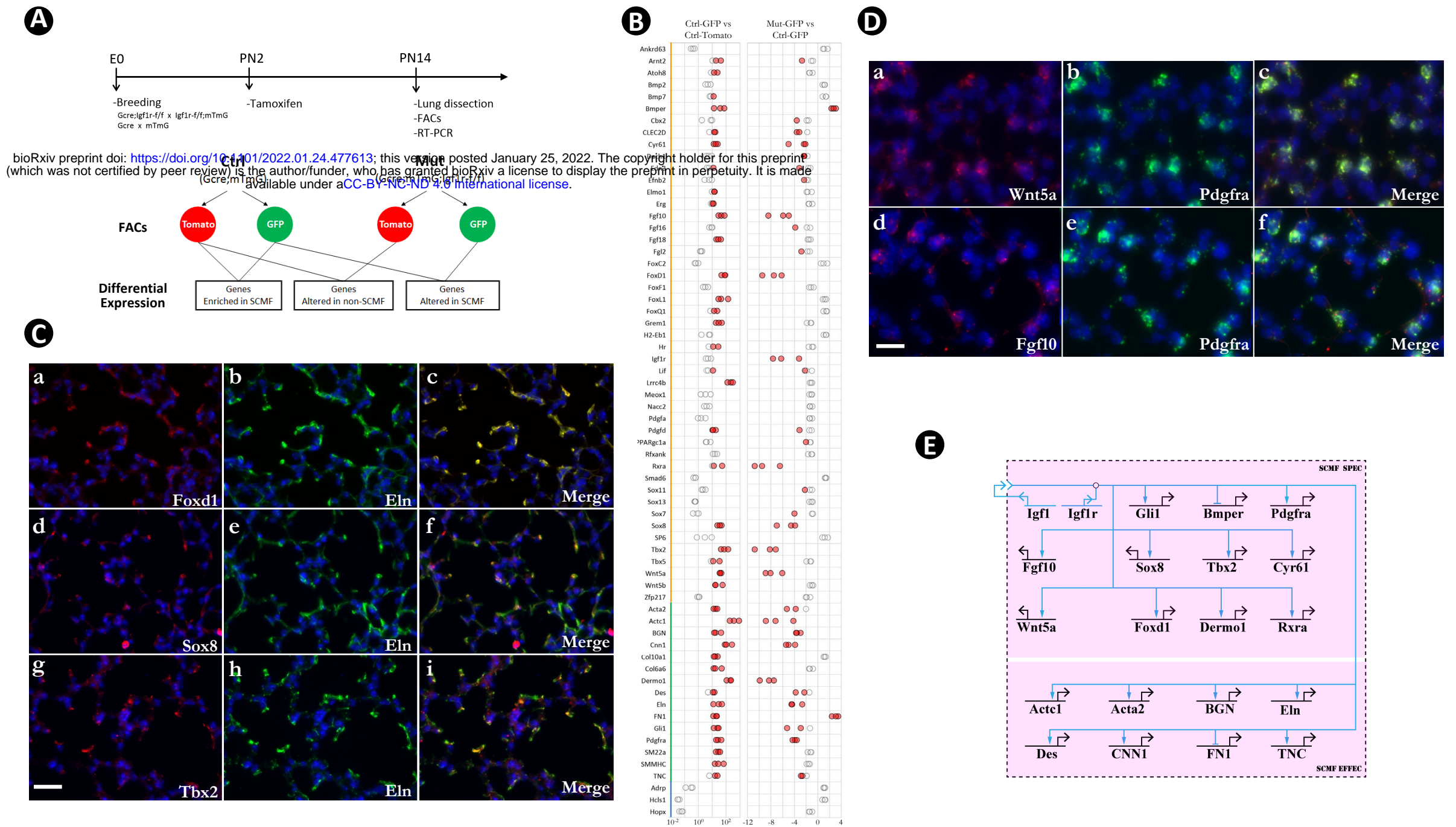


Figure 3: Identification of SCMF genes altered in *Gli1-cre^{ERT2};Igf1r-f/f* mutant lung. A: Schematic of the experimental protocol. B: RT-PCR data from the selected genes displaying their enrichment in SCMF and alterations in the mutant. Genes with orange line marked on their left: regulatory genes selected from LungMap database; Genes with green line: common SCMF markers; Genes with blue line: non-SCMF genes. Red circles: data points meeting the cutoff criteria described in the text, Empty circles: data points failing the cutoff criteria. This designation is used throughout the manuscript. C: Spatial expression of Foxd1 (a-c), SOX8 (d-f), and TBX2 (g-i) in the alveolar compartment of PN14 lungs as detected by immunostaining. Specific antibodies were used for SOX8 and TBX2, and RFP antibody was used for Foxd1 on lungs from Foxd1GCE;CAG^{Tomato} mice. Scale bar: 25um for all images. D: Spatial expression of Wnt5a (a-c) and Fgf10 (d-f) in the alveolar compartment of PN14 lungs as detected by RNAscope. Scale bar: 15um. E: Biotapestry network illustration of altered SCMF genes and their connections to Igf1 signaling. Genes (nodes) are shown in the territories (colored boxes) in which they are expressed. Edges show regulation by the originating upstream factor and are either positive (arrow) or repressive (bar). Signaling across cell membrane is indicated as double arrow heads.

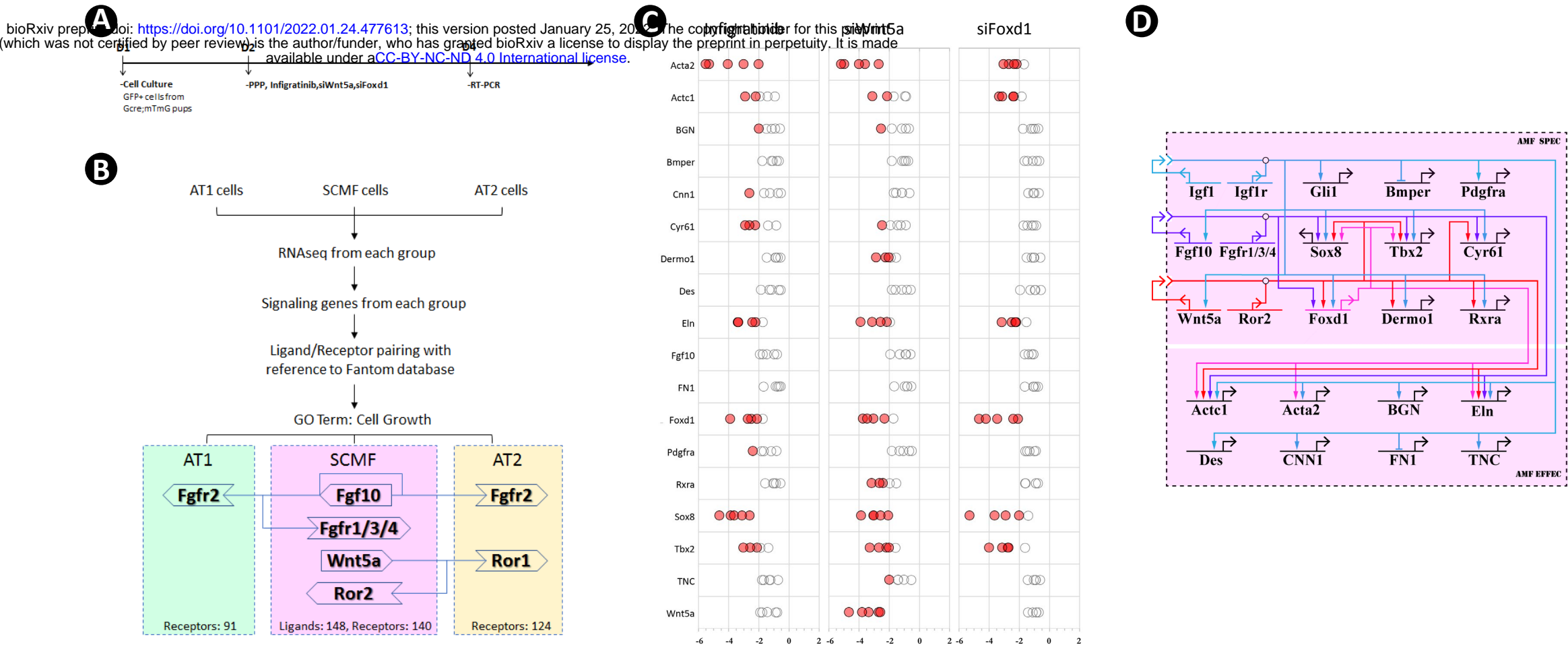


Figure 4: Cross regulation of the altered SCMF genes. A: Schematic of the experimental protocol. B: Flow chart of the secretome-receptome analysis among SCMF, AT1 and AT2 cells. The ligands and receptors were identified from the following RNAseq dataset with GLI1+ cells for SCMF (accession#: GSE126457 from Li et al., 2019), SFTPC+ cells for AT2 (accession#: GSE182886) and PDPN+ cells for AT1 (accession#: GSE106960 from Wang et al., 2018). C: RT-PCR data from the altered SCMF genes demonstrating their response to the treatments by Infigratinib, siWnt5a and siFoxd1. D: Biotapestry network illustration of the cross regulation among the altered SCMF genes.

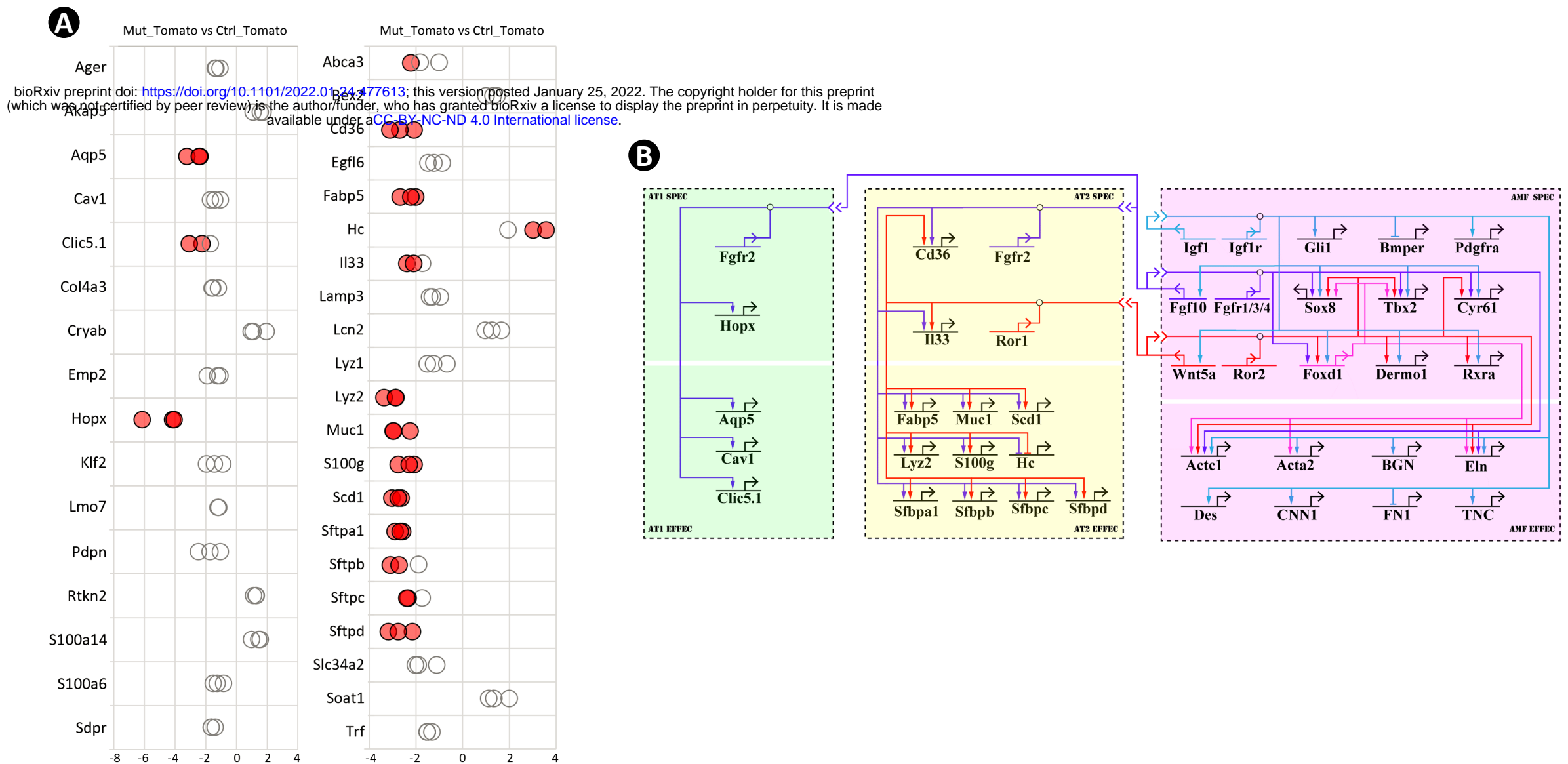


Figure 5: Epithelial genes affected in *Gli1-cre^{ERT2};Igf1r-f/f* mutant lung and their connections to SCMF Igf1 signaling. A: RT-PCR data from selected AT1 and AT2 genes revealing their alteration in the mutant lung. B: The Igf1 signaling GRN during alveologenesis with the IGF1 signaling-targeted epithelial genes and their cellular connections.

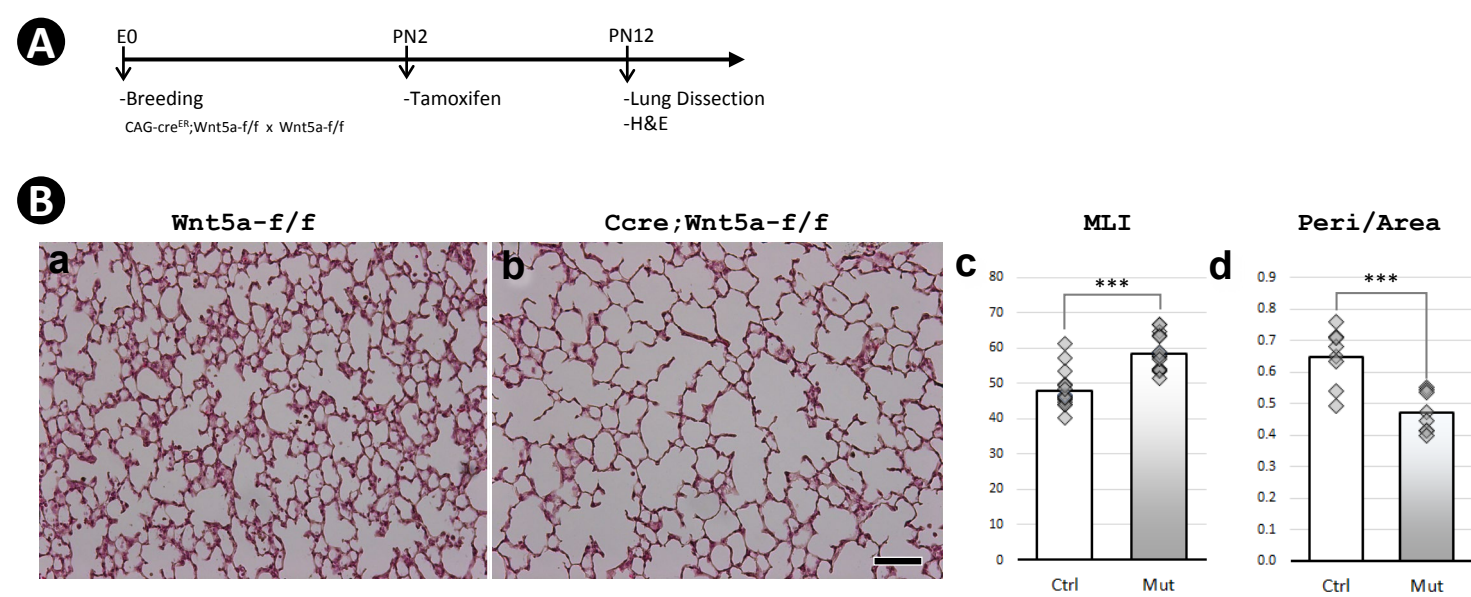


Figure 6: Postnatal inactivation of Wnt5a. A: Schematic of the experimental protocol. B: H&E staining of lung sections from control (a) and *Wnt5a*^{-/-} (b) mice and their morphometric measurements by MLI (c) and Peri/Area ratio (d). Scale bar: 100um for all images.

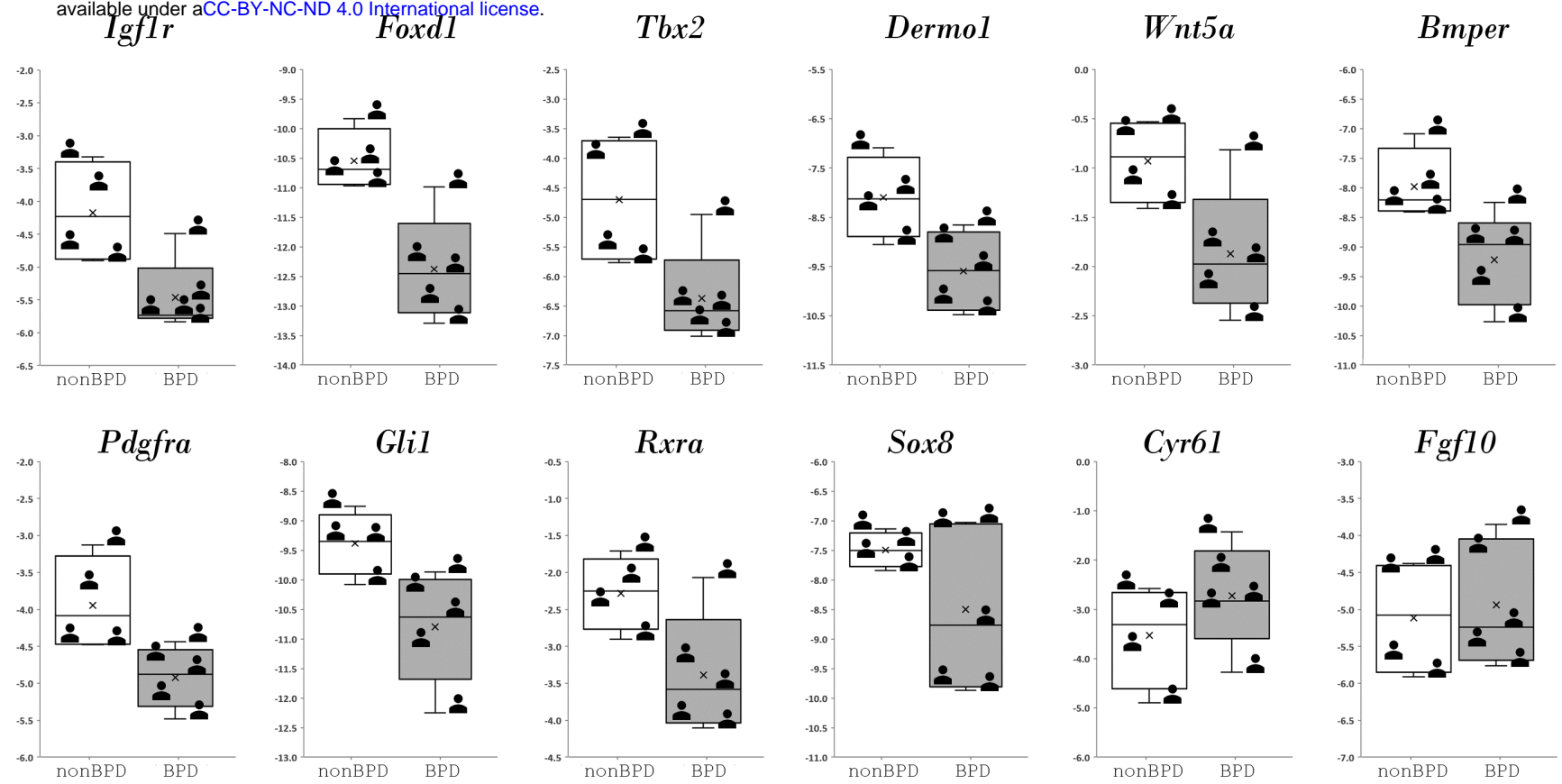


Figure 7: Regulatory genes from Igf1 signaling GRN and their expression in human bronchopulmonary dysplasia (BPD) lungs.

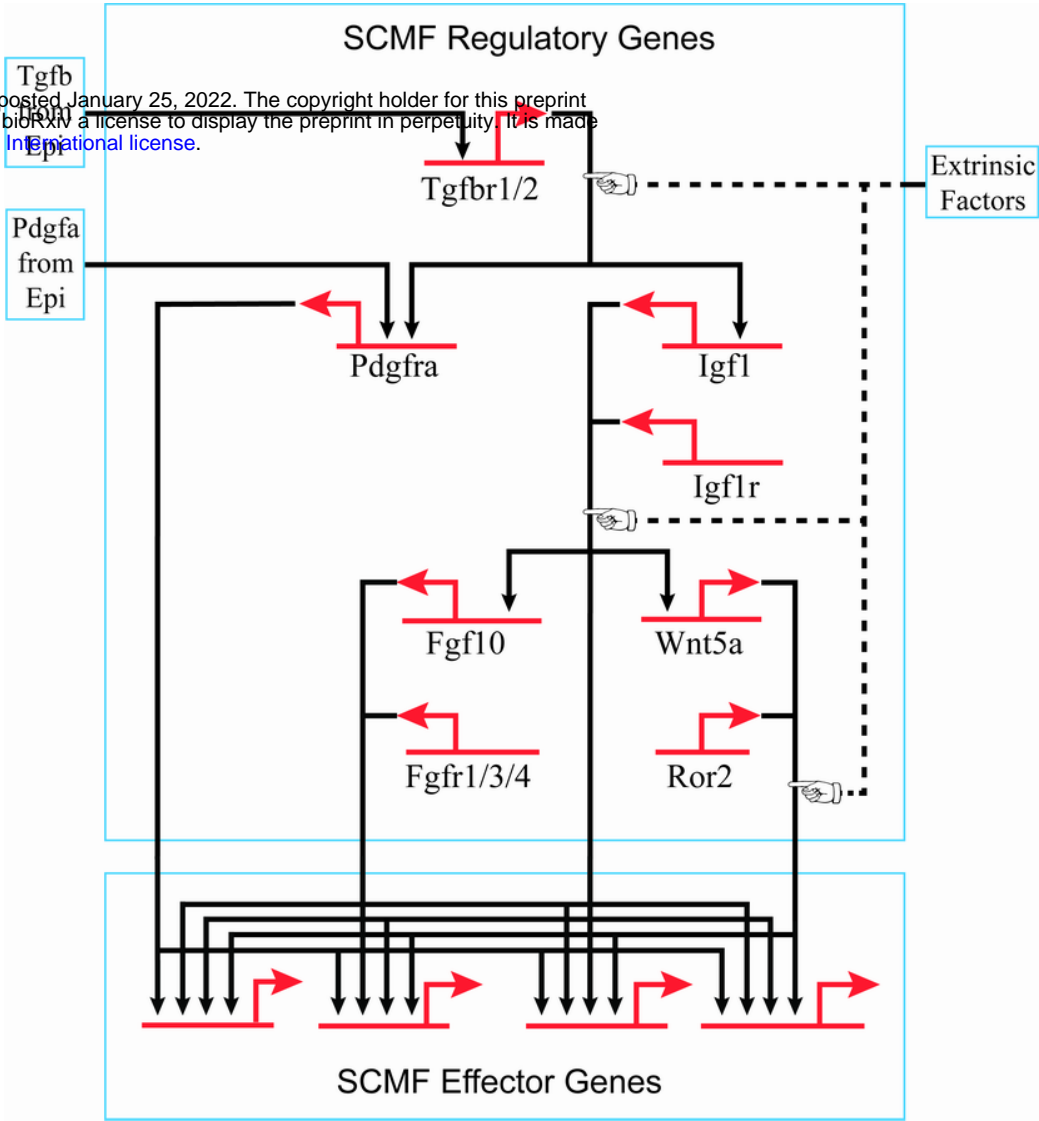
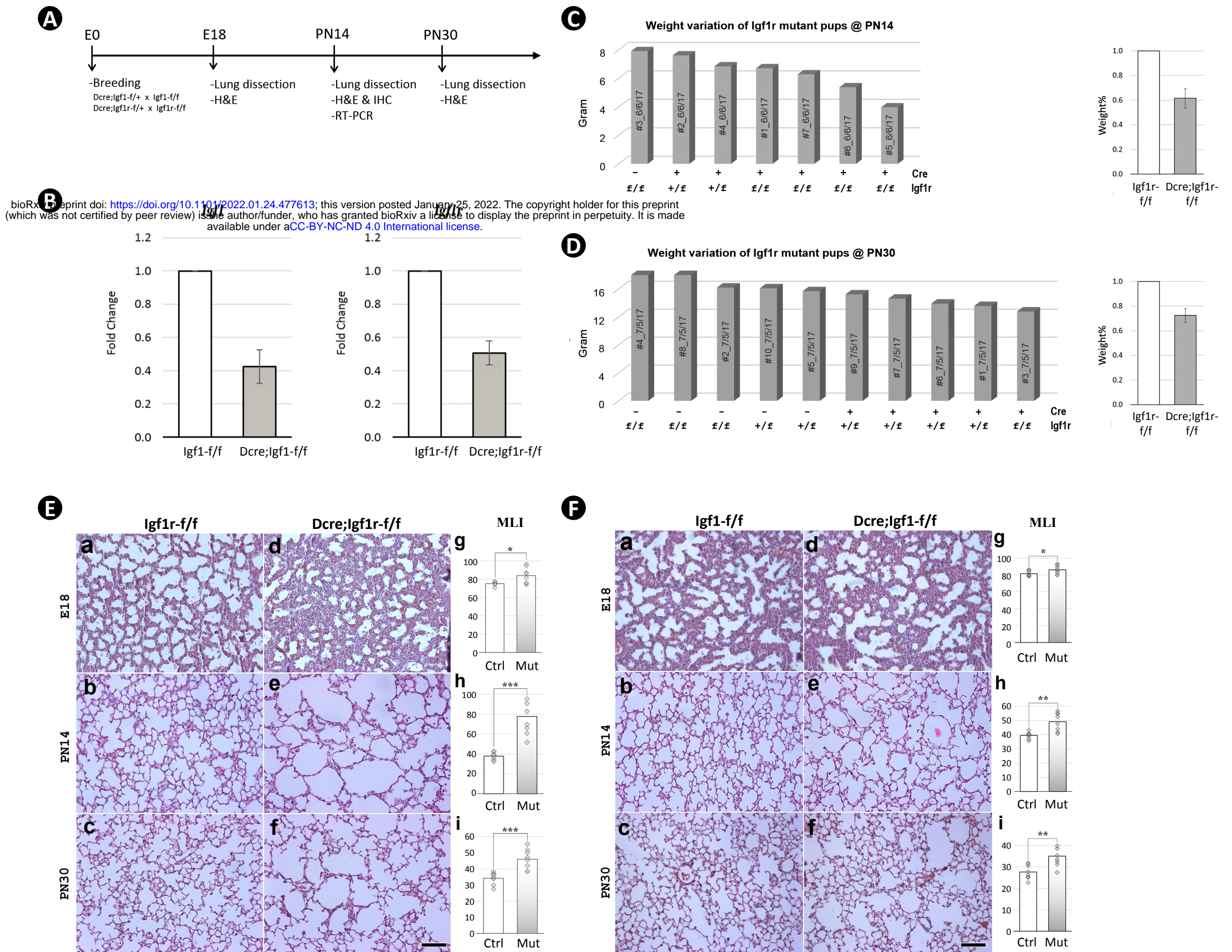
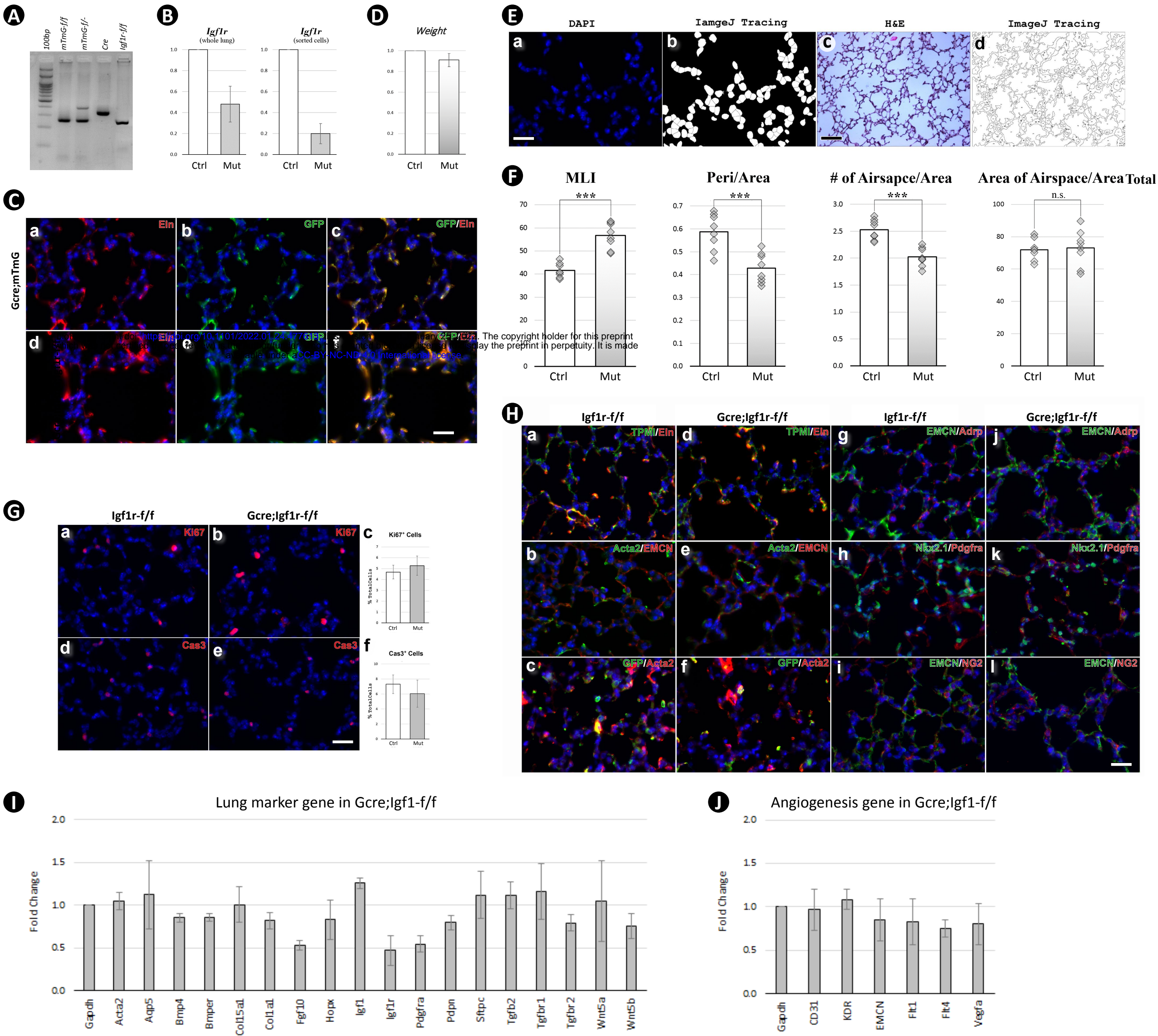


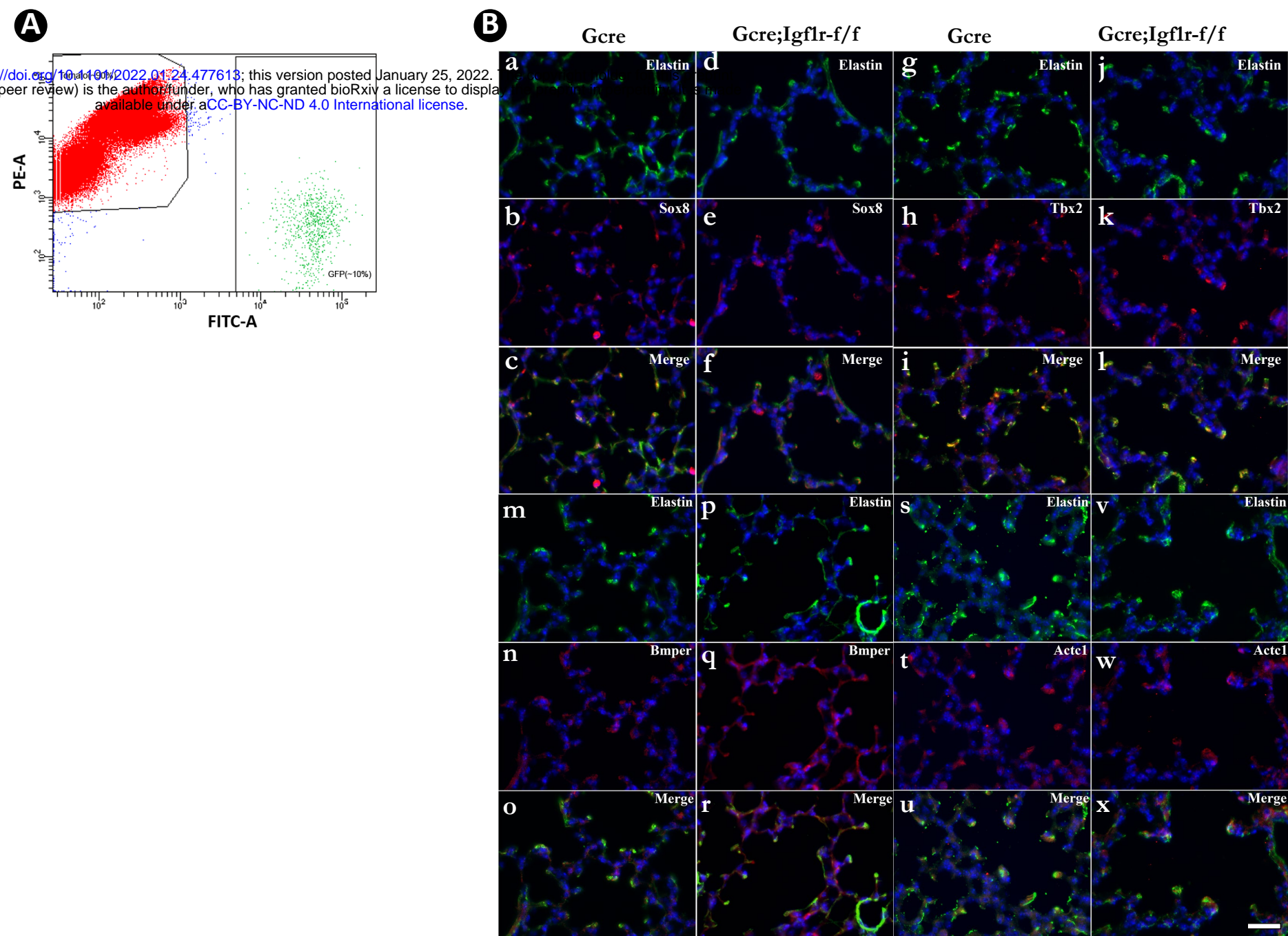
Figure 8: The hierarchical connections among the signaling pathways within SCMF during alveologenesis.



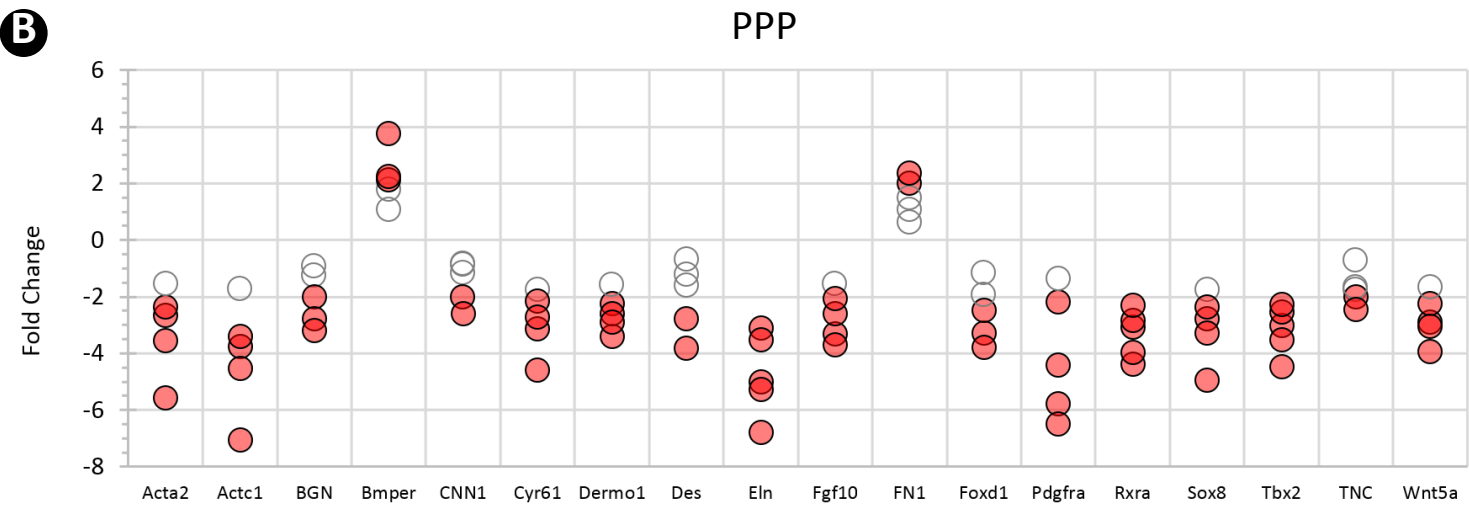
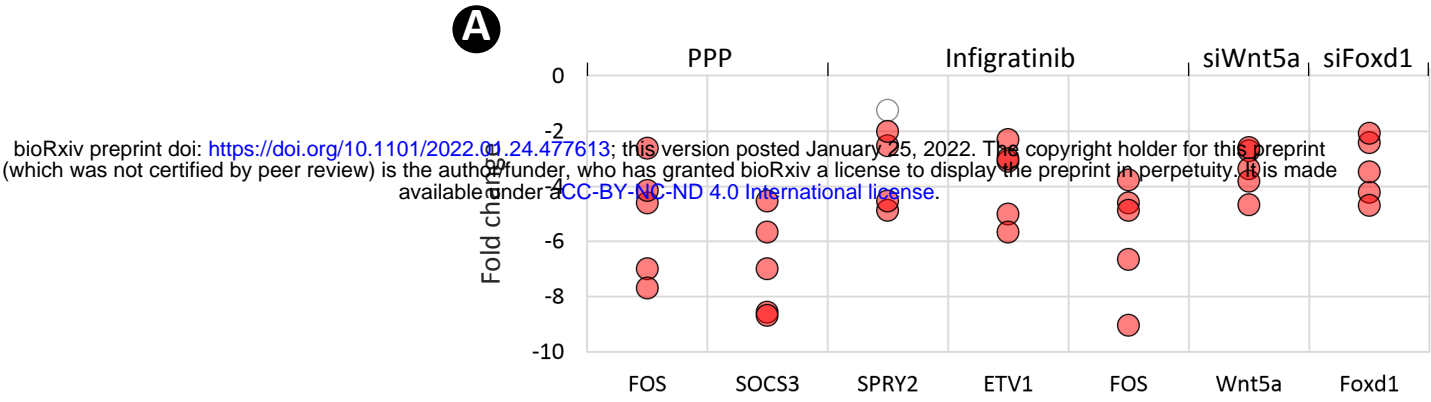
Supplemental Figure 1: Mesoderm constitutive deletion of Igf1 and Igf1r from mouse lung. A: Schematic of the experimental protocol. B: Impact of inactivation of Igf1 (left) and Igf1r (right) by Dermo1-cre on their respective transcripts in PN14 lungs. C: Body weight variation of pups at PN14 within a litter from the breeding of Dermo1-cre;lgf1r-f/- and Igf1r-f/f (left graph). Body weight comparison of pups from 4 litters between the control and the homozygous mutant (right graph). D: Same experiment as in E for pups at PN30. E: H&E staining of lung sections from Igf1r control (a-c) and Dermo1-cre mutant (d-f) mice and their morphometric measurements (g-i) at E18, PN14 and PN30. F: H&E staining of lung sections from Igf1 control (a-c) and Dermo1-cre mutant (d-f) mice and their morphometric measurements (g-i) at E18, PN14 and PN30. Scale bar: 100um for all images. *p*-value: * stands for 0.05-0.001, ** for 0.01-0.001, *** for <0.001, and the same designation is used through the paper.



Supplemental Figure 2: Postnatal inactivation of *Igf1r* in secondary crest myofibroblasts. A: genotyping of pups from the breeding between *Gli1-cre^{ERT2}*; *Igf1r-f/f* and *Igf1r-f/f*; *mTmG* mice. B: *Igf1r* expression in control and mutant lungs at PN14 using whole lung (left) and FACS sorted GFP+ cells (right). C: Immunostaining for Elastin and GFP on PN14 lung sections from *Gli1-cre^{ERT2}*; *mTmG* (a-c) and *Gli1-cre^{ERT2}*; *mTmG*; *Igf1r-f/f* (d-f) mice tamoxifen-treated at PN2. Scale bar: 25um for all images. D: Weight comparison between Ctrl and Mut at PN14. E: A sample of how to use ImageJ on cell counting (a,b) and morphometric measurements (c,d) where number of separated airspace (*N*), the perimeter (*Peri*) and area (*Area*) of each airspace can be calculated. Scale bar: 25um in a and 100um in c. F: Morphometric comparison between Ctrl and Mut at PN14 using different indexes. MLI is defined as in Crowley et al., 2019 and the others are quantified as below: $(Peri/Area) = \frac{\sum_1^N(Peri)}{\sum_1^N(Area)}$, $(\# of Airspace/Area) = \frac{N}{\sum_1^N(Area)}$, $(Area of Airspace/Area Total) = \frac{\sum_1^N(Area)}{(Area of the whole view field)}$. G: Immunostaining for Ki67 (a,b) and cleaved Caspase-3 (d,e) using control and mutant lungs at PN14, and comparison of the percentage of cells identified from their staining between control and mutant lungs (c,f). Scale bar: 25um for all images. H: Immunostaining for mesenchymal marker ELN (a,d), TPM1 (a,d), ACTA2 (b-f), PDGFRA (h,k), epithelial marker NKX2.1 (h,k), endothelial marker EMCN (b,e,g,j,i,l), lipofibroblast marker ADRP (g,j), and pericyte marker NG2 (i,l) using control and mutant lungs at PN14. Scale bar: 25um for all images. I: Comparative expression of selected lung marker genes between control and mutant lungs at PN14. J: Comparative expression of angiogenesis related genes between control and mutant lungs at PN14.



Supplemental Figure 3: Identification of SCMF genes altered in Gli1-cre^{ERT2};Igf1r-f/f mutant lung. A: GFP+ and Tomato+ cells are separated by FACS. B: Spatial expression of SOX8/ELN (a-f), TBX2/ELN (g-l), BMPER/ELN (m-r), and ACTC1/ELN (s-x) in the alveolar compartment in control and mutant lungs at PN14 as detected by immunostaining. Scale bar: 25um for all images.



Supplemental Figure 4: SCMF cell culture treatments. A: RT-PCR data showing the effect of various treatments (top) on their respective targeted genes (bottom). B: RT-PCR data from the altered SCMF genes demonstrating their response to the treatment from PPP.

Gene	Ctrl_GFP			Ctrl_Tomato			Mut_GFP			Level of expression in SCMF		Fold enrichment in SCMF					DE expression (fold change) in SCMF					Cellular expression in Lung						
	deltaCT to Gapdh			deltaCT to Gapdh			deltaCT to Gapdh			Ctrl_GFP	SEM	Ctrl_GFP/Ctrl_Tomato					Mut_GFP/Ctrl_GFP					Lungmap scRNAseq data						
	Mouse#1	Mouse#2	Mouse#3	Mouse#1	Mouse#2	Mouse#3	Mouse#1	Mouse#2	Mouse#3	Mean_deltaCT		#1/#1	#2/#2	#3/#3	Mean	p value	#1/#1	#2/#2	#3/#3	Mean	p value	SCMF	MatrixF8	LipoF8	Epi	Endo	tericyt	Immune
Ankrd63	-9.33	-9.25	-9.17	-7.98	-8.32	-7.39	-8.58	-9.18	-9.37	-9.25	4.62E-02	0.39	0.52	0.29	0.40	3.13E-02	1.68	1.05	-1.15	1.20	5.41E-01							
Arnt2	-6.55	-5.89	-7.24	-10.77	-11.27	-10.59	-8.00	-5.61	-7.41	-6.56	3.90E-01	18.64	41.64	10.20	23.49	1.81E-02	-2.73	1.21	-1.13	-1.22	4.80E-01							
Atoh8	-3.91	-2.40	-3.76	-6.91	-6.97	-7.51	-3.80	-2.85	-4.32	-3.36	4.80E-01	8.00	23.75	13.45	15.07	1.41E-02	1.08	-1.37	-1.47	-1.21	2.85E-01							
Bmp2	-8.70	-7.41	-9.58	-10.39	-9.64	-12.51	-8.43	-7.13	-10.33	-8.56	6.30E-01	3.23	4.69	7.62	5.18	2.38E-02	1.21	1.21	-1.68	1.00	8.63E-01							
Bmp7	-3.05	-3.18	-2.41	-6.01	-5.90	-6.04	-3.37	-2.67	-1.99	-2.88	2.38E-01	7.78	6.59	12.38	8.92	7.61E-03	0.80	1.42	1.34	1.19	5.20E-01							
Bmp7	-2.36	-2.47	-2.56	-7.58	-6.22	-8.79	-0.74	-1.28	-1.15	-2.46	5.78E-02	37.27	13.45	75.06	41.93	1.96E-02	3.07	2.29	2.66	2.67	7.55E-03							
Cbx2	-5.31	-5.52	-5.78	-8.27	-6.34	-9.04	-6.26	-7.37	-6.45	-5.54	1.36E-01	7.78	1.77	9.55	6.37	9.24E-02	-1.93	-3.61	-1.59	-2.11	8.31E-02							
CLEC2D	-10.12	-8.02	-8.99	-12.75	-12.09	-12.78	-10.98	-9.88	-10.81	-9.04	6.07E-01	6.19	16.80	13.83	12.27	1.55E-02	-1.82	-3.63	-3.53	-2.71	4.31E-02							
Cyr61	0.48	1.43	0.88	-3.24	-3.20	-3.29	-0.78	-0.90	-0.32	0.93	2.75E-01	13.18	24.76	18.00	18.65	3.94E-03	-2.39	-5.03	-2.30	-2.85	4.89E-02							
Dach1	-2.50	-2.00	-2.69	-4.34	-4.41	-5.85	-3.33	-3.22	-3.97	-2.40	2.06E-01	3.58	5.31	8.94	5.94	2.31E-02	-1.78	-2.32	-2.43	-2.14	1.57E-02							
Edn3	-5.98	-4.95	-5.63	-8.46	-6.97	-9.23	-6.69	-5.31	-7.30	-5.52	3.02E-01	5.58	4.06	12.13	7.25	2.89E-02	-1.64	-1.28	-3.18	-1.76	1.45E-01							
Efnb2	0.99	0.99	0.53	-1.54	-0.49	-2.68	0.23	-0.25	-0.43	0.84	1.53E-01	5.78	2.79	9.25	5.94	4.10E-02	-1.69	-2.37	-1.94	-1.96	1.95E-02							
Elmo1	-0.55	0.05	-0.12	-4.49	-3.18	-3.94	-0.64	-0.89	-0.90	-0.21	1.79E-01	15.31	9.38	14.12	12.94	3.54E-03	-1.07	-1.92	-1.72	-1.47	1.45E-01							
Erg	-6.37	-5.65	-6.80	-10.00	-8.67	-10.18	-6.28	-6.21	-7.47	-6.27	3.35E-01	12.38	8.11	10.41	10.30	2.79E-03	1.06	-1.47	-1.59	-1.27	2.50E-01							
Fgf10	-2.98	-1.46	-2.81	-7.82	-6.95	-9.10	-6.06	-3.78	-5.38	-2.42	4.81E-01	28.64	44.94	78.25	50.61	5.68E-03	-8.46	-4.99	-5.94	-6.16	7.01E-03							
Fgf16	-5.89	-4.45	-6.22	-9.00	-7.75	-8.80	-6.29	-5.36	-8.17	-5.52	5.43E-01	8.63	9.85	5.98	8.15	5.13E-03	-1.32	-1.88	-3.86	-1.94	1.40E-01							
Fgf18	-3.69	-2.69	-2.94	-8.02	-8.09	-7.70	-4.48	-3.01	-3.53	-3.11	3.00E-01	20.11	42.22	27.10	29.81	4.12E-03	-1.73	-1.25	-1.51	-1.47	5.32E-02							
Fgf2	-3.16	-1.42	-3.02	-3.55	-2.28	-3.63	-4.01	-2.93	-3.48	-2.53	5.58E-01	1.31	1.82	1.53	1.55	4.48E-02	-1.80	-2.84	-1.38	-1.84	9.16E-02							
FoxC2	-4.60	-4.80	-3.93	-3.71	-4.15	-3.88	-5.51	-4.88	-3.25	-4.44	2.63E-01	0.54	0.64	0.97	0.72	1.71E-01	-1.88	-1.06	1.60	1.03	8.43E-01							
Foxd1	-5.14	-3.24	-4.59	-10.67	-9.68	-10.94	-7.77	-6.49	-7.50	-4.32	5.64E-01	46.20	86.82	81.57	71.53	2.24E-03	-6.19	-9.51	-7.52	-7.51	3.72E-03							
FoxF1	-1.96	0.05	-1.73	-3.10	-2.26	-3.34	-2.52	-0.17	-1.27	-1.21	6.35E-01	2.20	4.96	3.05	3.41	3.83E-02	-1.47	-1.16	1.38	-1.03	7.56E-01							
Foxl1	-5.04	-3.75	-5.71	-10.48	-10.87	-10.52	-4.53	-3.99	-5.47	-4.83	5.75E-01	43.41	139.10	28.05	70.19	1.39E-02	1.42	-1.18	1.18	1.15	5.19E-01							
FoxO1	-4.69	-2.73	-4.49	-7.56	-7.24	-8.25	-4.73	-2.23	-3.83	-3.97	6.23E-01	7.31	22.78	13.55	14.55	1.59E-02	-1.03	1.41	1.58	1.32	2.24E-01							
Grem1	-3.46	-3.05	-4.24	-9.06	-7.25	-9.11	-3.78	-3.96	-4.42	-3.58	3.49E-01	48.50	18.38	29.24	32.04	6.77E-03	-1.25	-1.88	-1.13	-1.35	1.71E-01							
H2-Eb1	-8.86	-7.36	-8.92	-9.56	-9.92	-11.67	-8.43	-6.82	-8.92	-8.38	5.10E-01	1.62	5.90	6.73	4.75	9.21E-02	1.35	1.45	1.00	1.27	1.89E-01							
Hr	-4.12	-2.76	-4.98	-7.68	-7.56	-7.44	-4.75	-2.73	-4.69	-3.95	6.46E-01	11.79	27.88	5.50	15.05	3.34E-02	-1.55	1.02	1.22	-1.04	7.42E-01							
Irf1	-2.09	-0.25	-2.28	-4.39	-3.26	-4.09	-4.74	-1.94	-5.22	-1.54	6.47E-01	4.92	8.06	3.51	5.50	2.09E-02	-6.28	-3.23	-7.67	-5.00	2.34E-02							
Lif	-6.18	-6.07	-5.39	-8.12	-8.35	-8.87	-6.21	-7.21	-6.36	-5.88	2.47E-01	3.84	4.86	11.16	6.62	3.16E-02	-1.02	-2.21	-1.95	-1.54	1.74E-01							
Lrrc4b	-0.92	-0.33	-1.17	-7.93	-8.16	-9.45	-1.38	-0.56	-1.16	-0.81	2.49E-01	128.89	227.54	310.83	222.42	2.32E-03	-1.38	-1.17	1.01	-1.16	2.37E-01							
Meox1	-8.92	-8.29	-7.92	-9.46	-9.95	-10.81	-8.91	-8.36	-8.46	-8.38	2.92E-01	1.45	3.16	7.41	4.01	1.30E-01	1.01	-1.05	-1.45	-1.13	3.64E-01							
Nacc2	-4.89	-5.26	-5.92	-7.57	-7.20	-7.29	-5.39	-5.77	-5.84	-5.36	3.01E-01	6.41	3.84	2.58	4.28	3.42E-02	-1.41	-1.42	1.06	-1.22	2.55E-01							
Pdgfra	-4.96	-4.21	-4.84	-5.59	-4.11	-6.50	-4.92	-4.71	-5.38	-4.67	2.33E-01	1.55	0.93	3.16	1.88	2.89E-01	1.03	-1.41	-1.45	-1.24	2.16E-01							
Pdgfrd	-1.99	-1.59	-2.64	-6.14	-4.99	-6.12	-2.06	-3.24	-3.16	-2.07	3.06E-01	17.71	10.56	11.16	13.14	4.12E-03	-1.05	-3.14	-1.43	-1.52	2.53E-01							
PPARGc1a	-6.02	-4.36	-6.85	-7.94	-6.16	-9.70	-6.42	-4.79	-7.89	-5.74	7.32E-01	3.78	3.48	7.21	4.83	2.22E-02	-1.32	-1.35	-2.06	-1.51	9.60E-02							
Rfxank	-6.54	-6.23	-6.79	-10.47	-9.69	-11.25	-7.27	-6.30	-6.74	-6.52	1.62E-01	15.28	11.00	21.97	16.08	5.28E-03	-1.66	-1.05	1.04	-1.16	4.11E-01							
Rfxa	0.64	1.13	1.26	-3.07	-2.17	-4.42	-2.62	-2.30	-1.44	1.01	1.89E-01	13.09	9.85	51.27	24.73	2.89E-02	-9.55	-10.78	-6.50	-8.54	4.92E-03							
Smad6	-3.99	-3.67	-4.61	-3.34	-2.96	-3.40	-3.73	-3.11	-4.12	-4.09	2.76E-01	0.64	0.61	0.43	0.56	4.04E-02	1.20	1.47	1.40	1.36	4.05E-02							
Sox11	-7.17	-5.34	-7.18	-8.24	-7.04	-7.94	-8.31	-5.30	-7.63	-6.56	6.12E-01	2.10	3.25	1.69	2.35	5.10E-02	-2.20	1.03	-1.37	-1.36	2.70E-01							
Sox13	-5.74	-5.55	-6.16	-5.04	-4.74	-5.21	-5.85	-5.34	-6.68	-5.82	1.80E-01	0.62	0.57	0.52	0.57	7.69E-03	-1.08	1.16	-1.43	-1.08	5.76E-01							
Sox7	-4.26	-2.42	-5.40	-3.91	-2.41	-4.10	-3.98	-4.42	-5.45	-4.03	8.68E-01	0.78	0.99	0.41	0.73	2.88E-01	1.21	-4.00	-1.04	-1.23	4.94E-01							
Sox8	-3.25	-2.58	-3.87	-8.81	-7.14	-9.01	-5.45	-4.54	-6.68	-3.23	3.72E-01	47.18	23.59	35.26	35.34	3.23E-03	-4.59	-3.89	-7.01	-4.86	1.17E-02							
SP6	-9.48	-9.30	-8.41	-11.02	-8.94	-11.60	-9.25	-9.65	-7.64	-9.06	3.31E-01	2.91	0.78	9.13	4.27	2.91E-01	1.17	-1.27	1.71	1.22	5.72E-01							
Tbx2	3.39	4.50	3.32	-2.08</																								

Chemical	Concentration used in literature	Literature	Concentration tested	Concentration used in paper
PPP	0.1-10uM	Jin et al., 2018	0.5, 2, 4, 8 uM	4uM
	10uM	Chen et al., 2017		
	20uM	Wang et al., 2019		
Infigratinib	0.5uM	Nakamura et al., 2015	0.1, 1, 10 uM	1uM
	1.0uM	Wong et al., 2018		
	1.5uM	Manchado et al., 2016		
siWnt5a	20nM	Nemoto et al., 2012	10, 20, 40 nM	20nM
	20nM	Sakisaka et al., 2015		
	100nM	Zhao et al., 2017		
siFoxd1	20nM	Nakayama et al., 2015	10, 20, 40 nM	20nM
	20nM	Wu et al., 2018		
	100nM	Li et al., 2021		

Supplemental Table 2: List of the inhibitors and their concentrations used in cell culture treatment.

Supplemental Table 3. List of the primers used in the paper. Primers are for Mus musculus by default and for Homo sapiens when denoted with Hs.

Name	Sequence	Memo#1	Memo#2
Abca3-01	GGGCTGAGCTGTCCTTTATT	QPCR	Forward
Abca3-02	CCCAACTCCTTCTGCTTCTT	QPCR	Reverse
Acta2-01	CCATCATGCGTCTGGACTT	QPCR	Forward
Acta2-02	GGCAGTAGTCACGAAGGAATAG	QPCR	Reverse
Actc1-01	CCTCTCTGGAGAAGAGCTATGA	QPCR	Forward
Actc1-02	AATGAAAGAGGGCTGGAAGAG	QPCR	Reverse
Adrp-01	GAAGGATGTGGTGACGACTAC	QPCR	Forward
Adrp-02	TCACTGCTCCTTTGGTCTTATC	QPCR	Reverse
Ager-01	GTTGAGCCTGAAGGTGGAATAG	QPCR	Forward
Ager-02	AAGGGTGCAACCATCCTTTATC	QPCR	Reverse
Akap5-01	GGAGTCTTAGACACGGCTTTAC	QPCR	Forward
Akap5-02	CTCATAGGCCACAGAGCTAATG	QPCR	Reverse
Ankrd63-01	TTGGACAAGAGGGCTGATTATG	QPCR	Forward
Ankrd63-02	CCAGAAGGGAAGCTGGTAAA	QPCR	Reverse
Aqp5-01	GGCTGCAATCCTCTACTTCTAC	QPCR	Forward
Aqp5-02	TTCTTCCGCTCCTCTCTATGA	QPCR	Reverse
Arnt2-01	CTATGTCTTAACCTTGCCCATCC	QPCR	Forward
Arnt2-02	CTGAGCTCATGACCCTTCTTAC	QPCR	Reverse
Atoh8-01	CCATCCAGGGTTACTTCAGATT	QPCR	Forward
Atoh8-02	GGGCTCATCCATAATTTCTT	QPCR	Reverse
Bex2-01	CCAACTTCTGCCAGCTTCTA	QPCR	Forward
Bex2-02	TGAGCATCTTCCCATGCAATA	QPCR	Reverse
BGN-01	GTCCACTCAGAGACTCCCTATAA	QPCR	Forward
BGN-02	GCAGTGTGCTCTATCCATCTT	QPCR	Reverse
Bmp2-01	AGTAGTTTCCAGCACCGAATTA	QPCR	Forward
Bmp2-02	TTCATAACCTGGTGTCCAATAG	QPCR	Reverse
Bmp4-01	AACGTAGTCCCAAGCATCAC	QPCR	Forward
Bmp4-02	CGTCACTGAAGTCCACGTATAG	QPCR	Reverse
Bmp7-01	AGAGGTGGGATGTTGGTTATG	QPCR	Forward
Bmp7-02	CCAGTTTAACCTCTGCATTTG	QPCR	Reverse
Bmper-01	AGCGATGACCTTTGTTCTAGTC	QPCR	Forward
Bmper-02	GCAGAATCAGGCACACAAATAC	QPCR	Reverse
Bmper-Hs-01	AAGTGCAGGGCGTAATAGTG	QPCR	Forward
Bmper-Hs-02	CTGCAGATACGAGGGTGATTAG	QPCR	Reverse
CAG-creER-01	TAAAGATATCTCACGTACTGACGGTG	Genotyping_CAG-creER	Forward
CAG-creER-02	TCTCTGACCAGAGTCATCCTTAGC	Genotyping_CAG-creER	Reverse
CAG-Tomato-01	AAGGGAGCTGCAGTGGAGTA	Genotyping_CAG-Tomato	WT Forward
CAG-Tomato-02	CCGAAAATCTGTGGGAAGTC	Genotyping_CAG-Tomato	WT Reverse
CAG-Tomato-03	CTGTTCTGTACGGCATGG	Genotyping_CAG-Tomato	Mutant Forward
CAG-Tomato-04	GGCATTAAAGCAGCGTATCC	Genotyping_CAG-Tomato	Mutant Reverse
Cav1-01	ACTTCCCAGCTCACATTACAG	QPCR	Forward
Cav1-02	AGTCAAGCAGGGTTCCAATAC	QPCR	Reverse
Cbx2-01	ATGTCACAGCCAACCTCATC	QPCR	Forward
Cbx2-02	CTCGGGCAATGGTCTCAATAA	QPCR	Reverse
CD31-01	CACCCATCACTTACCACCTTATG	QPCR	Forward
CD31-02	TGTCTCTGGTGGGCTTATCT	QPCR	Reverse
Cd36-01	GGAGTGCTGGATTAGTGGTTAG	QPCR	Forward
Cd36-02	GCTGTGAGCAGACGTATAGAAG	QPCR	Reverse
CLEC2D-01	ATAGCCTCCACTGCCAAAC	QPCR	Forward
CLEC2D-02	GAAAGAGTAGCACCCACAGATAA	QPCR	Reverse
Clic5.1-01	GGAGGGATGGGAGGAAATAAAG	QPCR	Forward
Clic5.1-02	CTGATGTTGGAGTCTGCTCTAC	QPCR	Reverse
Cnn1-01	TTGAGAGAAGGCAGGAACATC	QPCR	Forward
Cnn1-02	GTACCCAGTTTGGGATCATAGAG	QPCR	Reverse

Coll0a1-01	CCCTGGTTCATGGGATGTTT	QPCR	Forward
Coll0a1-02	TGGCGTATGGGATGAAGTATTG	QPCR	Reverse
Coll5a1-01	TGCGTGTTTACCCAGTCATAG	QPCR	Forward
Coll5a1-02	AGGATTCTGTGCTGTTTCTCTC	QPCR	Reverse
Colla1-01	GCTTGAAGACCTATGTGGGTATAA	QPCR	Forward
Colla1-02	GGTGGAGAAAGGAGCAGAAA	QPCR	Reverse
Col4a3-01	CTGGCACTCTTAAGGTCATCTC	QPCR	Forward
Col4a3-02	GTCCAGGGTCTCCTTTTCATTC	QPCR	Reverse
Col6a6-01	GCTGAACCACCTGAAGAAGAA	QPCR	Forward
Col6a6-02	TTTGTGGGAGCAGAGAAATAGG	QPCR	Reverse
Cryab-01	TCTTCTCAACAGCCACTTCC	QPCR	Forward
Cryab-02	TCCTTCTCCAAACGCATCTC	QPCR	Reverse
Cyr61-01	CCAGTGACAGCAGCCTAAA	QPCR	Forward
Cyr61-02	CTGGAGCATCCTGCATAAGTAA	QPCR	Reverse
Cyr61-Hs-01	GAAGCAGCGTTTCCCTTCTA	QPCR	Forward
Cyr61-Hs-02	CTGACACTCTTCTCCCTTGTTT	QPCR	Reverse
Dach1-01	TCTAACTGGGCATGGACAAC	QPCR	Forward
Dach1-02	GGCCCTGTATGTTAGTGAGAAG	QPCR	Reverse
Dermol-01	CCAAGGCTCTCAGAACAAGAA	QPCR	Forward
Dermol-02	GGAGACGTAAAGAACAGGAGTATG	QPCR	Reverse
Dermol-cre-01	TAAAGATATCTCACGTACTGACGGTG	Genotyping_Dermol-cre	Forward
Dermol-cre-02	TCTCTGACCAGAGTCATCCTTAGC	Genotyping_Dermol-cre	Reverse
Dermol-Hs-01	AGACTCTGGTGCTGACTCTATC	QPCR	Forward
Dermol-Hs-02	CTGTGTCTCTTCTCCTCTCTAA	QPCR	Reverse
Des-01	TGACTCAGGCAGCCAATAAG	QPCR	Forward
Des-02	GCATCAATCTCGCAGGTGTA	QPCR	Reverse
Edn3-01	CGCTTGCGTTGTACTTGTATG	QPCR	Forward
Edn3-02	CTTTCTGCTCTCCCGGAATAA	QPCR	Reverse
Efnb2-01	AGAAGAGCAGAGAGCCAAATC	QPCR	Forward
Efnb2-02	ATCTGACCTGCCTTTCTTAATG	QPCR	Reverse
Egfl6-01	GCAAATGCAAGCAGGGATATAG	QPCR	Forward
Egfl6-02	CCCAGGTGCTGTGAGTATTT	QPCR	Reverse
Elmo1-01	CTAAGGCCAGGGTTGGATAAA	QPCR	Forward
Elmo1-02	CACATAGAGCTGATGGTGTGAG	QPCR	Reverse
Eln-01	CTGCCAAAGCTGCCAAATAC	QPCR	Forward
Eln-02	CCAACACCATAGCCAGGAAA	QPCR	Reverse
EMCN-01	CCCTACACCTGGGCAATAAA	QPCR	Forward
EMCN-02	GACTGGTGAGAAGACTGGAAAT	QPCR	Reverse
Emp2-01	GATGAGTCTGAGTGGCTTTAGG	QPCR	Forward
Emp2-02	GGAAGGAAGGAAAGGAGGATAG	QPCR	Reverse
Erg-01	CTGACCCAGCAGCTCATATT	QPCR	Forward
Erg-02	GATGCGGTCTCTCTGTCTTAG	QPCR	Reverse
Etv1-01	AAAGGTGGCTGGAGAAAGATAC	QPCR	Forward
Etv1-02	GTTATCCGGAAGGCCATAGAG	QPCR	Reverse
Fabp5-01	GCCAAGCCAGACTGTATCATTA	QPCR	Forward
Fabp5-02	CTCCCAGGTTACAAGAGAACAC	QPCR	Reverse
Fgf10-01	ATGCTGCCCTCTGGTTTAC	QPCR	Forward
Fgf10-02	AGAGAGAGAGAGAGAGAGAGAGA	QPCR	Reverse
Fgf10-Hs-01	ACTCTTCTTCTCCTCCTTCTC	QPCR	Forward
Fgf10-Hs-02	GACCTTCCCGTTCTTCTCAATC	QPCR	Reverse
Fgf16-01	GCCTCACAATCTACCCAGATAC	QPCR	Forward
Fgf16-02	ACACTTTCAGAGCTCTTTAG	QPCR	Reverse
Fgf18-01	GCGAGAACCAAGATGTA	QPCR	Forward
Fgf18-02	GCTTGGTGACTGTGGTGTAT	QPCR	Reverse
Fgl2-01	GAGACGCTCCATCTGGTAAAT	QPCR	Forward

Fgl2-02	GGAACACTTGCCATCCAAAC	QPCR	Reverse
Flt1-01	AGAGAGAGAGAGAGAGAGAGAGA	QPCR	Forward
Flt1-02	ACAGGGAAGGAATGGACTTTG	QPCR	Reverse
Flt4-01	CTAACCTGTCTGTGGGATTGAG	QPCR	Forward
Flt4-02	CGTAAGGGAGGGTTTGAGAAG	QPCR	Reverse
FN1-01	TCCTGTCTACCTCACAGACTAC	QPCR	Forward
FN1-02	GTCTACTCCACCGAACACAA	QPCR	Reverse
FOS-01	ATTGTCGAGGTGGTCTGAATG	QPCR	Forward
FOS-02	TCGAAAGACCTCAGGGTAGAA	QPCR	Reverse
FoxC2-01	TCTGTAAACGAGTGCGGATTT	QPCR	Forward
FoxC2-02	TGGGCAAGACGAAACCTTATC	QPCR	Reverse
Foxd1-01	TAGCTCAGAGGGTCCATCTATT	QPCR	Forward
Foxd1-02	AATTCCTAGTGCCAAGACAGAG	QPCR	Reverse
Foxd1GCE-01	TCTGGTCCAAGAATCCGAAG	Genotyping_Foxd1GCE	Common Reverse
Foxd1GCE-02	CTCCTCCGTGTCTCTCGTC	Genotyping_Foxd1GCE	WT Forward
Foxd1GCE-03	GGGAGGATTGGGAAGACAAT	Genotyping_Foxd1GCE	Mutant Forward
Foxd1-Hs-01	CTGTCCAGTGTGAGAACTTTA	QPCR	Forward
Foxd1-Hs-02	CGAACCACCAAGACGAGAAA	QPCR	Reverse
FoxF1-01	CATGTGTGACAGAAAGGAGTTTG	QPCR	Forward
FoxF1-02	GTGACCTGTCTGGTGATAGTAAG	QPCR	Reverse
Foxl1-01	TACTCCTGAGTGTGGGAGATAG	QPCR	Forward
Foxl1-02	CTGGAGGGATATAAAGGGAACAC	QPCR	Reverse
FoxQ1-01	GGCTTTCCTTTCCCTCCTATTT	QPCR	Forward
FoxQ1-02	GGAGTGGTTCCTGATGTATTT	QPCR	Reverse
Gapdh-01	GTGGCAAAGTGAGATTGTTG	QPCR	Forward
Gapdh-02	CGTTGAATTTGCCGTGAGTG	QPCR	Reverse
Gapdh-Hs-01	GGTGTGAACCATGAGAAGTATGA	QPCR	Forward
Gapdh-Hs-02	GAGTCCTTCCACGATACCAAG	QPCR	Reverse
Gli1-01	ACCACCTACCTCTGTCTATTC	QPCR	Forward
Gli1-02	TTCAGACCATTGCCATCAC	QPCR	Reverse
Gli1-creERT2-01	TAAAGATATCTCACGTACTGACGGTG	Genotyping_Gli1-creERT2	Forward
Gli1-creERT2-02	TCTCTGACCAGAGTCATCCTTAGC	Genotyping_Gli1-creERT2	Reverse
Gli1-Hs-01	AGCTAGAGTCCAGAGGTTCAA	QPCR	Forward
Gli1-Hs-02	TAGACAGAGGTTGGGAGGTAAG	QPCR	Reverse
Grem1-01	GTAACCTCTGAGGGCTGCATTAG	QPCR	Forward
Grem1-02	GATGTGAGGGAGAGCAAAGAAA	QPCR	Reverse
H2-Eb1-01	CAGATGTGGCAGGACAATAGA	QPCR	Forward
H2-Eb1-02	CCTTGAGCAGGCTGATTTAGA	QPCR	Reverse
Hc-01	GCTGACGCAGTCTGGATAAA	QPCR	Forward
Hc-02	CACAGTTTGGCCTGGAGAATA	QPCR	Reverse
Hcls1-01	CCGTAACCAGGAACCAGTAAAG	QPCR	Forward
Hcls1-02	CACAAAGTCAGGGTCTGTATCC	QPCR	Reverse
Hopx-01	GATGATGTGGGAACCGTCTT	QPCR	Forward
Hopx-02	CCCTGCCTGTTCTGTTATCTT	QPCR	Reverse
Hr-01	CTCTCCTTCCCCGGTCTCTATTA	QPCR	Forward
Hr-02	ATTTCTGCATTGCGCTTCTTTT	QPCR	Reverse
Igf1-01	CGGCAGGAGACATTTGATTTG	QPCR	Forward
Igf1-02	TCTTTCTCCTCTCTCCCTTCTT	QPCR	Reverse
Igf1-f/f-01	CACTAAGGAGTCTGTATTTGGACC	Genotyping_Igf1-f/f	Common Reverse
Igf1-f/f-02	AAACCACACTGCTCGACATTG	Genotyping_Igf1-f/f	Mutant Forward
Igf1-f/f-03	GGCAAATGGAAATCCTATGTCT	Genotyping_Igf1-f/f	WT Forward
Igf1r-03	GGAGGAGTTCGAGACAGAGTA	QPCR	Forward
Igf1r-04	CGATGCGGTACAGAGTGAAA	QPCR	Reverse
Igf1r-f/f-01	CTTCCCAGCTTGCTACTCTAGG	Genotyping_Igf1r-f/f	Forward
Igf1r-f/f-02	CAGGCTTGCAATGAGACATGGG	Genotyping_Igf1r-f/f	Reverse

Igf1r-Hs-01	TTCTCCCTTTCTCTCTCCTCTC	QPCR	Forward
Igf1r-Hs-02	GACAGCCACTTCTCAAAC	QPCR	Reverse
Il33-01	CCTACTCCCTCAGCTTTCTTTT	QPCR	Forward
Il33-02	GCAGGGTAAAGACAGTGAATA	QPCR	Reverse
KDR-01	GCGGAGACGCTCTTCATAATA	QPCR	Forward
KDR-02	GACAAGAAGGAGCCAGAAGAA	QPCR	Reverse
Klf2-01	GGCTAGATGCCTTGTGAGAAA	QPCR	Forward
Klf2-02	TGCCATCGTCTCCCTTATAGA	QPCR	Reverse
Lamp3-01	CCTAGTTCCTAGGCCTACTCTT	QPCR	Forward
Lamp3-02	CAATCAGTGCTAGTCCCATCTC	QPCR	Reverse
Lcn2-01	TCCTCAGGTACAGAGCTACAA	QPCR	Forward
Lcn2-02	GCTCCTTGGTTCTTCCATACA	QPCR	Reverse
Lif-01	CTGCTCTCCCTCTTTCTTTTC	QPCR	Forward
Lif-02	ACATTCCACAGGGTACATTC	QPCR	Reverse
Lmo7-01	CTCTCCCGTTCAATCGTTTCT	QPCR	Forward
Lmo7-02	CTCCTGTTATCCTCGTGTGTGT	QPCR	Reverse
Lrrc4b-01	ACAGGCAACTTCACCAGAG	QPCR	Forward
Lrrc4b-02	GCAAACCTCCCTTCAGTATCA	QPCR	Reverse
Lyz1-01	CAGCCCATCTGTCTCTTTCT	QPCR	Forward
Lyz1-02	TCTGCTGAAGTCTGTACTTG	QPCR	Reverse
Lyz2-01	ATGGAATGGCTGGCTACTATG	QPCR	Forward
Lyz2-02	GGTCTCCACGGTTGTAGTTT	QPCR	Reverse
Meox1-01	AACTCCAAAGGACTGGGAAAC	QPCR	Forward
Meox1-02	CAGAGGAGACCCTGATGTAAGA	QPCR	Reverse
Muc1-01	TACCTACCTACCACACTCAC	QPCR	Forward
Muc1-02	GAGAGACTGCTACTGCCATTAC	QPCR	Reverse
Nacc2-01	GTTAGGCCTCTACTGTGATGTG	QPCR	Forward
Nacc2-02	CACTGAAGAGGTCTCGGAAATAG	QPCR	Reverse
Pdgfa-01	TCCAGCGACTCTTGAGATA	QPCR	Forward
Pdgfa-02	TCTCGGGCACATGGTTAATG	QPCR	Reverse
Pdgfd-01	TAGAAATCCGCCGACTCAAC	QPCR	Forward
Pdgfd-02	GCACAGGAGAATGGAGACTAAA	QPCR	Reverse
Pdgfra-01	GACTTCCTAAAGAGTGACCATCC	QPCR	Forward
Pdgfra-02	CTTCCAGTCCTTCAGCTTATC	QPCR	Reverse
Pdgfra-Hs-01	GGAAACAGAAACCGAGGTATGA	QPCR	Forward
Pdgfra-Hs-02	CTGCATCGGGTCCACATAAA	QPCR	Reverse
Pdpn-01	GTCACCCTGGTTGGAATCATAG	QPCR	Forward
Pdpn-02	GGCGAGAACCTTCCAGAAAT	QPCR	Reverse
PPARgc1a-01	GACAATCCCGAAGACACTACAG	QPCR	Forward
PPARgc1a-02	AGAGAGGAGAGAGAGAGAGAGA	QPCR	Reverse
Rfxank-01	TTACCACCACACCCAAAGAC	QPCR	Forward
Rfxank-02	GACACCAATGCCCTTCAGATA	QPCR	Reverse
Rosa26-mTmG-01	TAGAGCTTGCGGAACCCTTC	Genotypin_Rosa26mTmG	Mutant Forward
Rosa26-mTmG-02	AGGGAGCTGCAGTGGAGTAG	Genotypin_Rosa26mTmG	WT Forward
Rosa26-mTmG-03	CTTTAAGCCTGCCCAGAAGA	Genotypin_Rosa26mTmG	Common Reverse
Rtnk2-01	TATAGGAAGCCGGGACTATGT	QPCR	Forward
Rtnk2-02	CTGCTCTGGCCTTTACCTATAC	QPCR	Reverse
Rxra-01	TCCGCAGGGAGTAAAGATAGA	QPCR	Forward
Rxra-02	CCATCCAGTTTACATGAGGGATAA	QPCR	Reverse
Rxra-Hs-01	GGACCCTCCTTTGGTGAAAT	QPCR	Forward
Rxra-Hs-02	AGGATTGGGAACGGCTAAAG	QPCR	Reverse
S100a14-01	CGAGCAACTGTGGGTTAGAA	QPCR	Forward
S100a14-02	CCTCTCCATCTTCACACTCTTG	QPCR	Reverse
S100a6-01	GCCTTGGCTTTGATCTACAATG	QPCR	Forward
S100a6-02	TAACCTACCCACCACTGGATTTG	QPCR	Reverse

S100g-01	AGAATGGCGATGGAGAAGTTAG	QPCR	Forward
S100g-02	CGTGCGTTCAATCAGTAGGT	QPCR	Reverse
Scd1-01	AGAGAGAGAGAGAGAGAGAGAGA	QPCR	Forward
Scd1-02	GGTTCAGAGGATGGACAGAAAG	QPCR	Reverse
Sdpr-01	CGGTGCTGATGGTAAGCTAATA	QPCR	Forward
Sdpr-02	TGGCATTCTTTGTTCTCCATTTC	QPCR	Reverse
Sftpa1-01	GGTGTCTAAGAAGCCAGAGAAC	QPCR	Forward
Sftpa1-02	CAAGATCCAGATCCAAGGAAGAG	QPCR	Reverse
Sftpb-01	TTGTCCACCTCCTCACAAAG	QPCR	Forward
Sftpb-02	GCAGCTTCAAGGAAGGATA	QPCR	Reverse
Sftpc-01	CAGACACCATCGCTACCTTT	QPCR	Forward
Sftpc-02	GTTCTGGAGCTGGCTTATAG	QPCR	Reverse
Sftpd-01	ACAATGGTGGAGCAGAGAAC	QPCR	Forward
Sftpd-02	GTGGCTCAGAACTCACAGATAA	QPCR	Reverse
Slc34a2-01	GAGTCAAGATGAAGCCAGTAGG	QPCR	Forward
Slc34a2-02	GGTATTACACGTGGGCTCTAAA	QPCR	Reverse
SM22a-01	CTAATGGCTTTGGGCAGTTTG	QPCR	Forward
SM22a-02	CTGTCTGTGAAGTCCCTCTTATG	QPCR	Reverse
Smad6-01	CGCACTTTGGCTTGTAATTCTT	QPCR	Forward
Smad6-02	GGCTTTCCACCTAGTTCTACTG	QPCR	Reverse
SMMHC-01	CTTCCTGGGCATTCTGGATATT	QPCR	Forward
SMMHC-02	CAGCTTCTCGTTGGTGTAGTT	QPCR	Reverse
Soat1-01	CTACAGCCATTTACGTTGTATTT	QPCR	Forward
Soat1-02	TTGCTCCCTCTCCCTCTTAT	QPCR	Reverse
SOCS3-01	GGTTCTGCTTTGTCTCTCTATG	QPCR	Forward
SOCS3-02	TCCCTCAACTCTCTGCCTATT	QPCR	Reverse
Sox11-01	CTACTGGCCAGGCTTCAATAA	QPCR	Forward
Sox11-02	ACGCCCACGTTACCATT	QPCR	Reverse
Sox13-01	CCATGACCAACCAGGAGAAA	QPCR	Forward
Sox13-02	AGGCCCTTGGCTTGTAATTATAG	QPCR	Reverse
Sox7-01	CTCCTGGGTACTGGGATTAAAG	QPCR	Forward
Sox7-02	CTGTAGTCGCCTGAGATGTATG	QPCR	Reverse
Sox8-01	TTGCTCTCCGGTTTGATAAG	QPCR	Forward
Sox8-02	TGAAGCCCATTTCTCTCCTTTG	QPCR	Reverse
Sox8-Hs-01	TCGTTAGGGCCTCAGTTCTA	QPCR	Forward
Sox8-Hs-02	AGGCGCTATTGTATGCTCTATG	QPCR	Reverse
SP6-01	CTGTCTGGACACGTCTTTAGTT	QPCR	Forward
SP6-02	CACCTCATCTCTGCTTTCTCTC	QPCR	Reverse
Spry2-01	CTGCTGCTGCTGATGGAATA	QPCR	Forward
Spry2-02	TAGGCATGCAGACCCAAATC	QPCR	Reverse
Tbx2-01	AGCGTAGACTTGAGCTAGGA	QPCR	Forward
Tbx2-02	GCTGATCCAGAAGTGACATAG	QPCR	Reverse
Tbx2-Hs-01	ACATCCTGAAGCTGCCTTAC	QPCR	Forward
Tbx2-Hs-02	AGCTGTGTGATCTTGTCTATTCT	QPCR	Reverse
Tbx5-01	AGAGAGAGAGAGAGAGAGAGAGA	QPCR	Forward
Tbx5-02	CTTGAGAGAGACTTGGAATCAG	QPCR	Reverse
Tgfb2-01	GGAACCACTGACCATTCTCTATT	QPCR	Forward
Tgfb2-02	CTGGCTTTCCCAAGGACTTTA	QPCR	Reverse
Tgfb1-01	GGGCTTAGTGTTCTGGGAAA	QPCR	Forward
Tgfb1-02	CCGATGGATCAGAAGGTACAAG	QPCR	Reverse
Tgfb2-01	CTGTGGGAGAAGTGAAGGATTAC	QPCR	Forward
Tgfb2-02	GTCTCTCAGCACACTGTCTTTC	QPCR	Reverse
TNC-01	CCAGGGTTGCCACCTATTT	QPCR	Forward
TNC-02	GTCTAGAGGATCCCACTCTACTT	QPCR	Reverse
Trf-01	CCCTCTGTGACCTGTGTATTG	QPCR	Forward

Trf-02	CTTTCTCAACGAGACACCTGAA	QPCR	Reverse
Vegfa-01	TGGTTCTTCACTCCCTCAAATC	QPCR	Forward
Vegfa-02	GGTCTCTCTCTCTCTTCTTGA	QPCR	Reverse
Wnt11-01	GGCTCACTTCAATCCCTCTTTA	QPCR	Forward
Wnt11-02	GGGCTTGCTCAGCATTTATTT	QPCR	Reverse
Wnt5a-01	GTCCCTTTGAGATGGGTGGTATC	QPCR	Forward
Wnt5a-02	TACCAGAGCACCTGCAATTC	QPCR	Reverse
Wnt5a-f/f-01	TGAGGGACTGGAAGTTGCAGG	Genotyping_Wnt5a-f/f	Forward
Wnt5a-f/f-02	TTCCAATGGGCTTCTGGAGAG	Genotyping_Wnt5a-f/f	Reverse
Wnt5a-Hs-03	TAAGCCCGGGAGTGGCTTTGG	QPCR	Forward
Wnt5a-Hs-04	GGGCGAAGGAGAAAAACGTGG	QPCR	Reverse
Wnt5b-01	AGAGTGCCAACACCAGTTT	QPCR	Forward
Wnt5b-02	CTCGGCTACCTATCTGCATAAC	QPCR	Reverse
Zfp217-01	GCTGGTAGAGCTAGAGCTAATG	QPCR	Forward
Zfp217-02	AGGCAACACCCACTCAAA	QPCR	Reverse